International Journal on Magnetic Particle Imaging
Vol 5, No 2, Article ID 1912001, 21 Pages

Infinite Science Publishing

Research Article

On the Representation of Magnetic Particle Imaging in Fourier Space

Marco Maass[a,*] · Alfred Mertins[a]

[a]Institute for Signal Processing, University of Lübeck, Lübeck, Germany
*Corresponding author, email: maass@isip.uni-luebeck.de

Received 12 December 2018; Accepted 20 November 2019; Published online 20 December 2019

Abstract

Magnetic particle imaging is a tracer-based medical imaging modality. Although various reconstruction methods are known, such as the ones based on a measured system matrix, the mathematical formulation of physical models of magnetic particle imaging is still lacking in several ways. Even for fairly simplified models, such as the Langevin model of paramagnetism, many properties are unproven. Only when one-dimensional excitation is used, the existing models are sufficient to derive simple and fast reconstruction techniques, like the so-called x-space and Chebyshev reconstruction approaches. Recently, an accurate formulation of the one-dimensional Fourier transform of the Langevin function and related functions has been provided. The present article extends the theory to multidimensional magnetic particle imaging. The derived formulations help us to calculate the exact relationship between the system function of Lissajous field-free-point trajectory based magnetic particle imaging and tensor products of Chebyshev polynomials and also uncover a direct relationship to tensor products of Bessel functions of first kind in the spatio-temporal Fourier domain. Moreover, the developed formulation consolidates the mathematical description of magnetic particle imaging and lays the basis for the investigation of different trajectories.

I. Introduction

Different mathematical models have been developed for magnetic particle imaging (MPI). A review can be found in [1]. However, the mathematical formulation of physical models in magnetic particle imaging still has several shortcomings. Even for simple models, many observations in MPI are unproven. For example, several MPI publications are based on the Langevin theory of paramagnetism to describe the imaging process [2–5]. However, although some reconstruction methods require the Fourier transform of the Langevin function and its derivative, in practice, due to the lack of a closed-form expression, they are approximated either numerically or via the Lorentzian function, which works quite well in practice. In a recent publication, we introduced a formal framework to explain MPI in spatio-temporal Fourier space for one-dimensional excitation [6]. In independent works [7, 8], closed-form solutions of the one-dimensional Fourier transform of the Langevin function can also be found. In [6], the Fourier transform has been defined on a highly simplified model in one dimension. The present article extends the previous results on one-dimensional MPI by giving further proofs and additional information, and, most importantly, extends the theory to the multidimensional case. The contributions of this work are manifold. First, the calculation of the Fourier transform of the Langevin function for the one-dimensional and the multidimensional case are presented. Then, a spatio-temporal Fourier representation of the system function is derived from a simplified Langevin model in the multidimensional setting that only depends on the spatial

Fourier transform of the Langevin function multiplied by a second function. This second function itself depends only on the selected field-free-point (FFP) trajectory and maps the spatial frequencies to temporal frequencies. As relevant examples, one-, two-, and three-dimensional excitation for the drive fields are used. In particular, to give an explicit example, Lissajous FFP-trajectories are used. This example helps us to prove some often assumed, but unproven relationships, like the one that the spatial dimensions of the system function components in MPI are related to tensor products of Chebyshev polynomials of second kind [2]. A second interesting observation is that the observed frequency mixing between spatial and temporal frequencies (see [9]) seems to originate within the calculated manifold conditions in the spatio-temporal Fourier space. This was so far related to the intermodulation theory in [2, 10]. Nonetheless, the techniques developed in this article can be extended to various FFP-trajectories and may be helpful in future for formal analyses in MPI. To confirm our findings numerically, simulations and comparisons between theoretical and experimental results have been performed.

II. The Langevin Function and its Role in MPI

The Langevin function plays a central role in the theory of MPI, as, for a given location of the field-free point, it allows one to derive a mathematical relationship between the SPIO distribution and the measured voltage signals. In this section, we recall some known results and introduce a normalized version of the Langevin function that will be useful in several proofs throughout the article.

The one-dimensional Langevin function $\mathscr{L}:\mathbb{R}\to\mathbb{R}$ with $\mathscr{L}\in L^\infty(\mathbb{R})$ is defined as

$$\mathscr{L}(x)=\begin{cases}\coth(x)-\frac{1}{x} & x\in\mathbb{R}\backslash\{0\},\\ 0 & x=0.\end{cases} \tag{1}$$

We introduce a "normalized" Langevin function $\mathscr{L}_{\mathrm{n}}:\mathbb{R}\to\mathbb{R}$ in the form

$$\mathscr{L}_{\mathrm{n}}(x)=\begin{cases}\frac{\mathscr{L}(x)}{x} & x\in\mathbb{R}\backslash\{0\},\\ \frac{1}{3} & x=0.\end{cases} \tag{2}$$

Finally, the n-dimensional Langevin function $\boldsymbol{\mathscr{L}}:\mathbb{R}^n\to\mathbb{R}^n$ is given by the expression

$$\boldsymbol{\mathscr{L}}(\boldsymbol{x})=\mathscr{L}(\|\boldsymbol{x}\|)\frac{\boldsymbol{x}}{\|\boldsymbol{x}\|}=\mathscr{L}_{\mathrm{n}}(\|\boldsymbol{x}\|)\boldsymbol{x}, \tag{3}$$

where $\|\cdot\|$ is the Euclidean norm of a vector.

For a simplified MPI model, in which no field inhomogeneities and no SPIO's relaxation effects are considered, the voltage signals caused by an n-dimensional SPIO distribution and received at n' receive coils can be written as a vector-valued T_D-periodic voltage function $\boldsymbol{u}:\mathbb{R}\to\mathbb{R}^{n'}$ [1, 2, 11]. We have

$$\boldsymbol{u}(t)=\boldsymbol{M}_0\boldsymbol{g}(t) \tag{4}$$

with $\boldsymbol{M}_0=\mu_0 m\boldsymbol{P}$, where matrix $\boldsymbol{P}\in\mathbb{R}^{n'\times n}$ denotes the homogeneous coil sensitivities profiles, μ_0 the vacuum permeability, m the magnetic moment of one nanoparticle, and $t\in\mathbb{R}$ denotes the time variable. The vector $\boldsymbol{g}:\mathbb{R}\to\mathbb{R}^n$ describes the essential content of the voltage signal $\boldsymbol{u}(t)$. Thus, for the reason of simplicity, we use only the auxiliary function $\boldsymbol{g}(t)$ instead of the voltage signals throughout the article. All upcoming results are related to the voltage signal $\boldsymbol{u}(t)$ through a linear transform with matrix $\boldsymbol{M}_0$. The function $\boldsymbol{g}(t)$ can be expressed by a component-wise integration using either $\mathscr{L}$, $\mathscr{L}_{\mathrm{n}}$ or $\boldsymbol{\mathscr{L}}$ as

$$\begin{aligned}\boldsymbol{g}(t)&=\frac{d}{dt}\int_{\mathbb{R}^n}c(\boldsymbol{x})\mathscr{L}(\beta\|\boldsymbol{G}(\boldsymbol{x}_{\mathrm{FFP}}(t)-\boldsymbol{x})\|)\\&\qquad\cdot\frac{\boldsymbol{G}(\boldsymbol{x}_{\mathrm{FFP}}(t)-\boldsymbol{x})}{\|\boldsymbol{G}(\boldsymbol{x}_{\mathrm{FFP}}(t)-\boldsymbol{x})\|}\,d\boldsymbol{x},\\&=\frac{d}{dt}\int_{\mathbb{R}^n}c(\boldsymbol{x})\mathscr{L}_{\mathrm{n}}(\beta\|\boldsymbol{G}(\boldsymbol{x}_{\mathrm{FFP}}(t)-\boldsymbol{x})\|)\\&\qquad\cdot\beta\boldsymbol{G}(\boldsymbol{x}_{\mathrm{FFP}}(t)-\boldsymbol{x})\,d\boldsymbol{x},\\&=\frac{d}{dt}\int_{\mathbb{R}^n}c(\boldsymbol{x})\boldsymbol{\mathscr{L}}(\beta(\boldsymbol{G}(\boldsymbol{x}_{\mathrm{FFP}}(t)-\boldsymbol{x})))\,d\boldsymbol{x}\end{aligned} \tag{5}$$

with $\beta=\frac{\mu_0 m}{k_B T}$. The vector $\boldsymbol{x}\in\mathbb{R}^n$ denotes the spatial position, $c:\mathbb{R}^n\to\mathbb{R}$ is the spatial SPIO distribution, k_B the Boltzmann constant, and T the temperature of the SPIOs. The matrix $\boldsymbol{G}\in\mathbb{R}^{n\times n}$ denotes the applied gradients of the selection field $\boldsymbol{H}^S(\boldsymbol{x})=\boldsymbol{G}\boldsymbol{x}$. The vector $\boldsymbol{x}_{\mathrm{FFP}}:\mathbb{R}\to\mathbb{R}^n$ describes the position of the field free point at time t.

Often the relationship in (5) is written in an alternative form as an inner product between the SPIO distribution $c(\boldsymbol{x})$ and a system function $\boldsymbol{s}:\mathbb{R}^n\times\mathbb{R}\to\mathbb{R}^n$ that includes all terms that are independent of $c(\boldsymbol{x})$:

$$\boldsymbol{g}(t)=\int_{\mathbb{R}^n}\boldsymbol{s}(\boldsymbol{x},t)c(\boldsymbol{x})\,d\boldsymbol{x}. \tag{6}$$

A comparison with (5) shows that the system function itself can be written in the following forms:

$$\begin{aligned}\boldsymbol{s}(\boldsymbol{x},t)&=\frac{\partial}{\partial t}\left[\mathscr{L}(\beta\,\|\boldsymbol{G}(\boldsymbol{x}_{\mathrm{FFP}}(t)-\boldsymbol{x})\|)\frac{\beta\boldsymbol{G}(\boldsymbol{x}_{\mathrm{FFP}}(t)-\boldsymbol{x})}{\|\beta\boldsymbol{G}(\boldsymbol{x}_{\mathrm{FFP}}(t)-\boldsymbol{x})\|}\right]\\&=\frac{\partial}{\partial t}\left[\mathscr{L}_{\mathrm{n}}(\beta\,\|\boldsymbol{G}(\boldsymbol{x}_{\mathrm{FFP}}(t)-\boldsymbol{x})\|)\beta\boldsymbol{G}(\boldsymbol{x}_{\mathrm{FFP}}(t)-\boldsymbol{x})\right]\\&=\frac{\partial}{\partial t}\left[\boldsymbol{\mathscr{L}}(\beta(\boldsymbol{G}(\boldsymbol{x}_{\mathrm{FFP}}(t)-\boldsymbol{x})))\right].\end{aligned} \tag{7}$$

Another common approach is to define an MPI system function for the Fourier-series representation of the T_D-periodic function $\boldsymbol{g}(t)$. With

$$\boldsymbol{s}_k(\boldsymbol{x})=\frac{1}{T_D}\int_{-\frac{T_D}{2}}^{\frac{T_D}{2}}\boldsymbol{s}(\boldsymbol{x},t)\mathrm{e}^{-\mathrm{i}\omega_k t}\,dt \tag{8}$$

being the k-th Fourier series component of the system function $\boldsymbol{s}(\boldsymbol{x},t)$, the frequency-domain version of (6) reads

$$\begin{aligned}\boldsymbol{g}_k &= \frac{1}{T_D}\int_{-\frac{T_D}{2}}^{\frac{T_D}{2}} \boldsymbol{g}(t)\mathrm{e}^{-\mathrm{i}\omega_k t}\,dt \\ &= \int_{\mathbb{R}^n} \boldsymbol{s}_k(\boldsymbol{x})c(\boldsymbol{x})\,d\boldsymbol{x}\end{aligned} \tag{9}$$

with $\omega_k = \frac{2\pi k}{T_D} = 2\pi k f_D$.

III. Spatial Fourier transform

As a first fundamental result on the relationship between the FFP trajectory and the series coefficients $\boldsymbol{g}_k$, we show that SPIO- and trajectory-dependent terms can be separated when carrying out a spatial Fourier transform.

Theorem 3.1. *The Fourier series coefficients $\boldsymbol{g}_k$ of $\boldsymbol{g}(t)$ in (9) can be expressed in terms of the spatial Fourier transform by*

$$\boldsymbol{g}_k = \frac{\mathrm{i}\omega_k}{(2\pi)^n}\int_{\mathbb{R}^n} \hat{\boldsymbol{h}}(\boldsymbol{\omega}_x)P(\boldsymbol{\omega}_x,k)\,d\boldsymbol{\omega}_x, \tag{10}$$

where the function

$$P(\boldsymbol{\omega}_x,k) = \frac{1}{2\pi}\int_{-\pi}^{\pi} \mathrm{e}^{\mathrm{i}\boldsymbol{\omega}_x^T \boldsymbol{x}_{\mathrm{FFP}}\left(\frac{z}{2\pi f_D}\right)}\mathrm{e}^{-\mathrm{i}kz}\,dz \tag{11}$$

only depends on the used FFP-trajectory $\boldsymbol{x}_{\mathrm{FFP}}(t)$ with period length $T_D = \frac{1}{f_D}$. The term $\hat{\boldsymbol{h}}(\boldsymbol{\omega}_x)$ is given by

$$\hat{\boldsymbol{h}}(\boldsymbol{\omega}_x) = \hat{c}(\boldsymbol{\omega}_x)\frac{1}{\left|\det(\beta\boldsymbol{G})\right|}\hat{\mathscr{L}}\left(\frac{\boldsymbol{G}^{-T}\boldsymbol{\omega}_x}{\beta}\right), \tag{12}$$

where $\hat{\mathscr{L}}(\boldsymbol{\omega}_x)$ and $\hat{c}(\boldsymbol{\omega}_x)$ are the continuous Fourier transforms of the Langevin function $\mathscr{L}(\boldsymbol{x})$ and the SPIO distribution, respectively. Let $c(\boldsymbol{x})$ be of bounded support and in $L^1(\mathbb{R}^n)\cap L^2(\mathbb{R}^n)$.

Proof. In the following, a vector-valued notation is used:

$$\boldsymbol{h}(\boldsymbol{x}) = \int_{\mathbb{R}^n} c(\boldsymbol{u})\mathscr{L}\left(\beta\boldsymbol{G}(\boldsymbol{x}-\boldsymbol{u})\right)\,d\boldsymbol{u}. \tag{13}$$

We are now interested in the Fourier series expansion of $\frac{d}{dt}\boldsymbol{h}(\boldsymbol{x}_{\mathrm{FFP}}(t))$. Its coefficients are given by

$$\begin{aligned}\boldsymbol{g}_k &= f_D\int_{-\frac{T_D}{2}}^{\frac{T_D}{2}}\left[\frac{d}{dt}\boldsymbol{h}(\boldsymbol{x}_{\mathrm{FFP}}(t))\right]\mathrm{e}^{-\mathrm{i}\omega_k t}\,dt \\ &= \mathrm{i}\omega_k f_D\int_{-\frac{T_D}{2}}^{\frac{T_D}{2}} \boldsymbol{h}(\boldsymbol{x}_{\mathrm{FFP}}(t))\mathrm{e}^{-\mathrm{i}\omega_k t}\,dt,\end{aligned} \tag{14}$$

where $\omega_k = 2\pi f_k = 2\pi\frac{k}{T_D} = 2\pi k f_D$ with T_D being the duration of one period of the FFP over the whole trajectory.

The convolution in (13) is equivalent to a multiplication in Fourier space for each vector component:

$$\hat{\boldsymbol{h}}(\boldsymbol{\omega}_x) = \hat{c}(\boldsymbol{\omega}_x)\frac{1}{\left|\det(\beta\boldsymbol{G})\right|}\hat{\mathscr{L}}\left(\frac{\boldsymbol{G}^{-T}\boldsymbol{\omega}_x}{\beta}\right). \tag{15}$$

A formal proof of this has to be performed within the distribution theory. As $c(\boldsymbol{x})$ has a bounded support, is in $L^1(\mathbb{R}^n)\cap L^2(\mathbb{R}^n)$, and the locally integrable function $\mathscr{L}(\boldsymbol{x})$ is in $L^\infty(\mathbb{R}^n)$, the integral in (13) exists and $\boldsymbol{h}(\boldsymbol{x})$ is locally integrable. The latter makes it possible to define a distributional forward Fourier transform on $\boldsymbol{h}(\boldsymbol{x})$, which is given by $\hat{\boldsymbol{h}}(\boldsymbol{\omega}_x)$ in (15).

Following the idea in [12], $\boldsymbol{h}(\boldsymbol{x}_{\mathrm{FFP}}(t))$ is represented by the inverse Fourier transform along $\boldsymbol{\omega}_x$:

$$\boldsymbol{h}(\boldsymbol{x}_{\mathrm{FFP}}(t)) = \frac{1}{(2\pi)^n}\int_{\mathbb{R}^n}\hat{\boldsymbol{h}}(\boldsymbol{\omega}_x)\mathrm{e}^{\mathrm{i}\boldsymbol{\omega}_x^T\boldsymbol{x}_{\mathrm{FFP}}(t)}\,d\boldsymbol{\omega}_x. \tag{16}$$

Now, by substituting $t = \frac{z}{2\pi f_D}$ in (14), inserting (16), and changing the order of integration, we obtain

$$\begin{aligned}\boldsymbol{g}_k &= \frac{\mathrm{i}\omega_k}{2\pi}\int_{-\pi}^{\pi}\boldsymbol{h}\left(\boldsymbol{x}_{\mathrm{FFP}}\left(\frac{z}{2\pi f_D}\right)\right)\mathrm{e}^{-\mathrm{i}kz}\,dz \\ &= \frac{\mathrm{i}\omega_k}{(2\pi)^{n+1}}\int_{-\pi}^{\pi}\int_{\mathbb{R}^n}\hat{\boldsymbol{h}}(\boldsymbol{\omega}_x)\mathrm{e}^{\mathrm{i}\boldsymbol{\omega}_x^T\boldsymbol{x}_{\mathrm{FFP}}\left(\frac{z}{2\pi f_D}\right)}\,d\boldsymbol{\omega}_x\,\mathrm{e}^{-\mathrm{i}kz}\,dz \\ &= \frac{\mathrm{i}\omega_k}{(2\pi)^n}\int_{\mathbb{R}^n}\hat{\boldsymbol{h}}(\boldsymbol{\omega}_x)\left[\frac{1}{2\pi}\int_{-\pi}^{\pi}\mathrm{e}^{\mathrm{i}\boldsymbol{\omega}_x^T\boldsymbol{x}_{\mathrm{FFP}}\left(\frac{z}{2\pi f_D}\right)}\mathrm{e}^{-\mathrm{i}kz}\,dz\right]d\boldsymbol{\omega}_x.\end{aligned} \tag{17}$$

The comparison of (17) with (10) and (11) confirms the theorem. □

IV. Fourier transform of the Langevin function and Bessel functions

In this section, we provide results on the Fourier transforms of the Langevin function and some related functions which naturally occur in the MPI context. Readers who are mainly interested in MPI theory may skip most of this section and consider only the derived Fourier correspondences.

IV.I. Transform of the Langevin function

The expression for the Fourier transform of the Langevin function is derived on the basis of a series expansion for $\mathscr{L}(x)$ which is stated in the following lemma.

Lemma 4.1. *The Langevin function $\mathscr{L}:\mathbb{R}\to\mathbb{R}$ has the uniformly converging series expansion*

$$\mathscr{L}(x) = \sum_{k=1}^{\infty}\frac{2x}{k^2\pi^2+x^2} = \frac{1}{\mathrm{i}}\sum_{k=1}^{\infty}\left(\frac{1}{k\pi-\mathrm{i}x}-\frac{1}{k\pi+\mathrm{i}x}\right). \tag{18}$$

10.18416/ijmpi.2019.1912001

Consequently, the normalized version $\mathcal{L}_\mathrm{n}:\mathbb{R}\to\mathbb{R}$ has the uniformly converging series expansion

$$\mathcal{L}_\mathrm{n}(x)=\sum_{k=1}^{\infty}\frac{2}{k^2\pi^2+x^2}. \tag{19}$$

The proofs of the uniform convergence are deferred to Appendix A.

Theorem 4.2. *The one-dimensional Fourier transform of the normalized Langevin function $\mathcal{L}_\mathrm{n}:\mathbb{R}\to\mathbb{R}$ is given by*

$$\hat{\mathcal{L}}_\mathrm{n}(\omega_x)=-2\ln\left(1-\mathrm{e}^{-\pi|\omega_x|}\right),\quad |\omega_x|>0 \tag{20}$$

with $\hat{\mathcal{L}}_\mathrm{n}\in L^1(\mathbb{R})$.

Proof. From Lemma 4.1, we have

$$\begin{aligned}\hat{\mathcal{L}}_\mathrm{n}(\omega_x)&=\mathscr{F}\left[\mathcal{L}_\mathrm{n}(x)\right]\\&=\mathscr{F}\left[\sum_{k=1}^{\infty}\frac{2}{k^2\pi^2+x^2}\right]=\sum_{k=1}^{\infty}\mathscr{F}\left[\frac{2}{k^2\pi^2+x^2}\right].\end{aligned}$$

Using the fact that the Fourier transform of $\frac{2}{k^2\pi^2+x^2}$ is given by

$$\mathscr{F}\left[\frac{2}{k^2\pi^2+x^2}\right]=\frac{2}{k}\mathrm{e}^{-k\pi|\omega_x|}$$

and that [13]

$$\sum_{k=1}^{\infty}\frac{1}{k}z^{-k}=-\ln\left(1-\frac{1}{z}\right)\quad\text{for}\quad |z|>1,$$

we obtain

$$\hat{\mathcal{L}}_\mathrm{n}(\omega_x)=\sum_{k=1}^{\infty}\frac{2}{k}\mathrm{e}^{-k\pi|\omega_x|}=-2\ln\left(1-\mathrm{e}^{-\pi|\omega_x|}\right),\quad |\omega_x|>0. \tag{21}$$

Next we show that $\hat{\mathcal{L}}_\mathrm{n}$ is in $L^1(\mathbb{R})$. Due to the singularity around $\omega_x=0$ and the property that $\hat{\mathcal{L}}_\mathrm{n}(\omega_x)$ is symmetric and non-negative for all ω_x, the integration over $|\hat{\mathcal{L}}_\mathrm{n}|$ is performed by taking limits in the following form:

$$\int_{-\infty}^{\infty}\left|\hat{\mathcal{L}}_\mathrm{n}(\omega_x)\right|d\omega_x=2\lim_{\epsilon^+\to 0}\int_{\epsilon}^{\frac{1}{\epsilon}}\hat{\mathcal{L}}_\mathrm{n}(\omega_x)d\omega_x.$$

Using the series expansion in (21) and the fact that the series is convergent for all $\omega_x>0$, the limit and the integration can be interchanged. We thus have

$$\begin{aligned}\int_{-\infty}^{\infty}\left|\hat{\mathcal{L}}_\mathrm{n}(\omega_x)\right|d\omega_x&=2\lim_{\epsilon^+\to 0}\int_{\epsilon}^{\frac{1}{\epsilon}}\sum_{k=1}^{\infty}\frac{2}{k}\mathrm{e}^{-k\pi\omega_x}d\omega_x\\&=2\lim_{\epsilon^+\to 0}\sum_{k=1}^{\infty}\int_{\epsilon}^{\frac{1}{\epsilon}}\frac{2}{k}\mathrm{e}^{-k\pi\omega_x}d\omega_x\\&=2\lim_{\epsilon^+\to 0}\sum_{k=1}^{\infty}\frac{-2}{\pi k^2}\mathrm{e}^{-k\pi\omega_x}\Big|_{\epsilon}^{\frac{1}{\epsilon}}\\&=2\sum_{k=1}^{\infty}\left(\frac{-2}{\pi k^2}\mathrm{e}^{-k\pi\infty}-\frac{-2}{\pi k^2}\mathrm{e}^{-k\pi 0}\right)\\&=2\sum_{k=1}^{\infty}\frac{2}{\pi k^2}=\frac{2\pi}{3}<\infty.\end{aligned}$$

□

In the following, we extend the one-dimensional correspondence between $\mathcal{L}_\mathrm{n}(x)$ and $\hat{\mathcal{L}}_\mathrm{n}(\omega_x)$ to higher dimensions. For this purpose it is helpful to introduce the terminology of radial functions. These provide a straightforward way to perform integration of a radial function in spherical coordinates.

Definition. *A function $f:\mathbb{R}^n\to\mathbb{C}$ is a radial (rotational invariant) function if there is a one-dimensional function $F:\mathbb{R}_+\to\mathbb{C}$ such that*

$$f(\boldsymbol{x})=F(\|\boldsymbol{x}\|). \tag{22}$$

From this definition it is easy to conclude that the function $\ell_\mathrm{n}:\mathbb{R}^n\to\mathbb{R}$ with $\ell_\mathrm{n}(\boldsymbol{x})=\mathcal{L}_\mathrm{n}(\|\boldsymbol{x}\|)$ is a radial function.

Lemma 4.3. *If $f:\mathbb{R}^n\to\mathbb{C}$ with $f(\boldsymbol{x})=F(\|\boldsymbol{x}\|)$ is a radial function, then the following identity holds*

$$\int_{\mathbb{R}^n}F(\|\boldsymbol{x}\|)d\boldsymbol{x}=S_{n-1}\int_0^{\infty}F(r)r^{n-1}\,dr, \tag{23}$$

where

$$S_{n-1}=\frac{2\pi^{\frac{n}{2}}}{\Gamma\left(\frac{n}{2}\right)}$$

denotes the surface of the unit $(n-1)$-dimensional sphere.

A proof can be found in [14].

Theorem 4.4. *The three-dimensional Fourier transform of $\ell_\mathrm{n}:\mathbb{R}^3\to\mathbb{R}$ with $\ell_\mathrm{n}(\boldsymbol{x})=\mathcal{L}_\mathrm{n}(\|\boldsymbol{x}\|)$ results in*

$$\hat{\mathcal{L}}_\mathrm{n}(\boldsymbol{\omega_x})=\Lambda_3(s)\qquad\text{with}\qquad s=\|\boldsymbol{\omega_x}\| \tag{24}$$

and

$$\Lambda_3(s)=\frac{4\pi^2}{s}\frac{1}{\mathrm{e}^{\pi s}-1}. \tag{25}$$

Proof. In [15, 16] a connection between different dimensionalities of the Fourier transform of a radial function was derived. Assuming that $\hat{f}_n(s)$ with $s:\mathbb{R}^n\to\mathbb{R}$ and $s(\boldsymbol{\omega_x})=\|\boldsymbol{\omega_x}\|$ denotes the n-dimensional Fourier transform of a radial function $f(r)$, then the $n+2$ dimensional Fourier transform can be calculated by

$$\hat{f}_{n+2}(s)=-\frac{2\pi\hat{f}_n'(s)}{s}.$$

Now using our result from Theorem 4.2 and setting $\Lambda_1(s)=-2\ln(1-\mathrm{e}^{-\pi s})$ we obtain for the three-dimensional case

$$\Lambda_3(s)=-\frac{2\pi}{s}\Lambda_1'(s)=2\frac{2\pi}{s}\frac{\pi\mathrm{e}^{-\pi s}}{1-\mathrm{e}^{-\pi s}}=\frac{4\pi^2}{s}\frac{1}{\mathrm{e}^{\pi s}-1}.$$

This confirms (24) and (25). □

Note that also a characterization of the two-dimensional Fourier transform of the normalized Langevin function is available. However, since the 2-D case has no closed-form solution and since this result is not needed to prove Theorem 4.4, it is deferred to Appendix E.

10.18416/ijmpi.2019.1912001

Lemma 4.5. *The three-dimensional Fourier transform of the normalized Langevin function $\mathcal{L}_{\mathrm{n}} : \mathbb{R}^3 \to \mathbb{R}$ is in $L^1(\mathbb{R}^3)$.*

Proof. According to Lemma 4.3 for radial functions we have

$$\int_{\mathbb{R}^3} \left|\hat{\mathcal{L}}_{\mathrm{n}}(\boldsymbol{\omega}_{\boldsymbol{x}})\right| \, d\boldsymbol{\omega}_{\boldsymbol{x}} = 4\pi \int_0^\infty \Lambda_3(r) r^2 \, dr = 16\pi^3 \int_0^\infty \frac{r}{\mathrm{e}^{\pi r} - 1} \, dr.$$

By performing the substitution $s = \pi r$ and using just the definition of the product of the gamma function $\Gamma(x)$ and the zeta function $\zeta(x)$ [13],

$$\Gamma(x)\zeta(x) = \int_0^\infty \frac{t^{x-1}}{\mathrm{e}^t - 1} \, dt,$$

we obtain

$$\int_{\mathbb{R}^3} \left|\hat{\mathcal{L}}_{\mathrm{n}}(\boldsymbol{\omega}_{\boldsymbol{x}})\right| \, d\boldsymbol{\omega}_{\boldsymbol{x}} = 16\pi \int_0^\infty \frac{s}{\mathrm{e}^s - 1} \, ds = 16\pi\Gamma(2)\zeta(2) = \frac{8\pi^3}{3} < \infty.$$

□

The fact that $\hat{\mathcal{L}}_{\mathrm{n}}(\boldsymbol{\omega}_{\boldsymbol{x}}) \in L^1(\mathbb{R}^3)$ means that there exists an inverse Fourier transform

$$\mathcal{L}_{\mathrm{n}}(\|\boldsymbol{x}\|) = \frac{1}{(2\pi)^3} \int_{\mathbb{R}^3} \hat{\mathcal{L}}_{\mathrm{n}}(\boldsymbol{\omega}_{\boldsymbol{x}}) \mathrm{e}^{\mathrm{i}\boldsymbol{\omega}_{\boldsymbol{x}}^T \boldsymbol{x}} \, d\boldsymbol{\omega}_{\boldsymbol{x}},$$

where $\hat{\mathcal{L}}_{\mathrm{n}}(\boldsymbol{\omega}_{\boldsymbol{x}}) = \Lambda_3(\|\boldsymbol{\omega}_{\boldsymbol{x}}\|)$. This also allows us to define a forward and inverse Fourier transform $\hat{\boldsymbol{\mathcal{L}}}(\boldsymbol{\omega}_{\boldsymbol{x}})$ for the n-dimensional Langevin function. The forward transform is formulated in the next theorem.

Theorem 4.6. *The Fourier transform of $\boldsymbol{\mathcal{L}} : \mathbb{R}^n \to \mathbb{R}^n$ is*

$$\hat{\boldsymbol{\mathcal{L}}}(\boldsymbol{\omega}_{\boldsymbol{x}}) = \mathrm{i}\Lambda_n'(\|\boldsymbol{\omega}_{\boldsymbol{x}}\|) \frac{\boldsymbol{\omega}_{\boldsymbol{x}}}{\|\boldsymbol{\omega}_{\boldsymbol{x}}\|}, \tag{26}$$

with $\hat{\boldsymbol{\mathcal{L}}} : \mathbb{R}^n \to \mathbb{C}^n$, $\Lambda_n'(s) = \frac{d}{ds}\Lambda_n(s)$, and $\Lambda_n : \mathbb{R}_+ \to \mathbb{R}$ denoting the n-dimensional Fourier transform of $\mathcal{L}_{\mathrm{n}}(\|\boldsymbol{x}\|)$:

$$\Lambda_n(\|\boldsymbol{\omega}_{\boldsymbol{x}}\|) = \hat{\mathcal{L}}_{\mathrm{n}}(\boldsymbol{\omega}_{\boldsymbol{x}}) = \mathcal{F}[\mathcal{L}_{\mathrm{n}}(\|\boldsymbol{x}\|)].$$

The function $\Lambda_n(s)$ has been derived for different n in this work. For $n = 1$ it is given by $\Lambda_1(s) = \hat{\mathcal{L}}_{\mathrm{n}}(s)$ in (20), for $n = 2$ the result is shown in Appendix E in (106), and for $n = 3$ it is given by (25).

Proof. We start from the n-dimensional formulation of the Langevin function $\boldsymbol{\mathcal{L}}(\boldsymbol{x})$ in (3). Observing that it has the form $\mathcal{L}_{\mathrm{n}}(\|\boldsymbol{x}\|)\boldsymbol{x}$ and using the Fourier correspondence $(-\mathrm{i}x)f(x) \longleftrightarrow \frac{d}{d\omega}\hat{f}(\omega)$ for a derivative in frequency domain leads to the correspondence

$$\boldsymbol{\mathcal{L}}(\boldsymbol{x}) = \mathcal{L}_{\mathrm{n}}(\|\boldsymbol{x}\|)\boldsymbol{x} \longleftrightarrow \mathrm{i}\nabla_{\boldsymbol{\omega}_{\mathrm{x}}} \hat{\mathcal{L}}_{\mathrm{n}}(\boldsymbol{\omega}_{\boldsymbol{x}}),$$

where $\nabla_{\boldsymbol{\omega}_{\mathrm{x}}} = \left[\frac{\partial}{\partial\omega_{x_1}}, \frac{\partial}{\partial\omega_{x_2}}, \ldots, \frac{\partial}{\partial\omega_{x_n}}\right]^T$ is the gradient operator with respect to $\boldsymbol{\omega}_{\boldsymbol{x}}$. Considering that $\hat{\mathcal{L}}_{\mathrm{n}}(\boldsymbol{\omega}_{\boldsymbol{x}}) = \Lambda_n(\|\boldsymbol{\omega}_{\boldsymbol{x}}\|)$ and applying the chain-rule, the Fourier transform of $\boldsymbol{\mathcal{L}}(\boldsymbol{x})$ finally becomes

$$\hat{\boldsymbol{\mathcal{L}}}(\boldsymbol{\omega}_{\boldsymbol{x}}) = \mathcal{F}[\boldsymbol{\mathcal{L}}(\boldsymbol{x})] = \mathrm{i}\nabla_{\boldsymbol{\omega}_{\mathrm{x}}}[\Lambda_n(\|\boldsymbol{\omega}_{\boldsymbol{x}}\|)] = \mathrm{i}\Lambda_n'(\|\boldsymbol{\omega}_{\boldsymbol{x}}\|)\frac{\boldsymbol{\omega}_{\boldsymbol{x}}}{\|\boldsymbol{\omega}_{\boldsymbol{x}}\|},$$

which proves (26). □

Finally, the explicit expression for the Fourier transform of the three-dimensional Langevin function is given in the following corollary.

Corollary 4.7. *The 3D Fourier transform of $\boldsymbol{\mathcal{L}} : \mathbb{R}^3 \to \mathbb{R}^3$ is*

$$\hat{\boldsymbol{\mathcal{L}}}(\boldsymbol{\omega}_{\boldsymbol{x}}) = -4\pi^2\mathrm{i}\frac{(\pi\|\boldsymbol{\omega}_{\boldsymbol{x}}\| + 1)\,\mathrm{e}^{\pi\|\boldsymbol{\omega}_{\boldsymbol{x}}\|} - 1}{\|\boldsymbol{\omega}_{\boldsymbol{x}}\|^2\,(\mathrm{e}^{\pi\|\boldsymbol{\omega}_{\boldsymbol{x}}\|} - 1)^2} \frac{\boldsymbol{\omega}_{\boldsymbol{x}}}{\|\boldsymbol{\omega}_{\boldsymbol{x}}\|}. \tag{27}$$

Quite obviously, in a physical context, the Langevin function $\boldsymbol{\mathcal{L}}(\boldsymbol{x})$ has to be treated in a three-dimensional way due to the three-dimensional structure of SPIO distributions. However, it is not clear under which conditions $\hat{\boldsymbol{\mathcal{L}}}(\boldsymbol{\omega}_{\boldsymbol{x}})$ may be used inside an argument of an inverse Fourier transform. To verify this, the following Lemma helps.

Lemma 4.8. *Products of the form*

$$\omega_{x_1}^{\ell}\omega_{x_2}^{m}\omega_{x_3}^{n}\hat{\mathcal{L}}_{\nu}(\boldsymbol{\omega}_{\boldsymbol{x}}), \qquad \ell, m, n \in \mathbb{N}_0, \tag{28}$$

where $\hat{\mathcal{L}}_{\nu} : \mathbb{R}^3 \to \mathbb{C}$, $\nu \in \{1,2,3\}$ are the components of $\hat{\boldsymbol{\mathcal{L}}}(\boldsymbol{\omega}_{\boldsymbol{x}})$, are in $L^1(\mathbb{R}^3)$ if $\ell + m + n \geq 1$.

The proof of this lemma, which is quite technical, is given in Appendix B. The important point about the lemma is that it shows that an inverse Fourier transform exists as soon as $\hat{\boldsymbol{\mathcal{L}}}(\boldsymbol{\omega}_{\boldsymbol{x}})$ occurs in a product with a second function $f(\boldsymbol{\omega}_{\boldsymbol{x}})$ for which $\frac{1}{\omega_{x_i}} f(\boldsymbol{\omega}_{\boldsymbol{x}}) \in L^1(\mathbb{R}^3) \cap L^\infty(\mathbb{R}^3)$. Interestingly, Bessel functions of first kind with an order that is higher than zero are of this type. These functions naturally occur in Fourier-domain representations of the MPI measurement process.

IV.II. Fourier Transforms of Bessel functions

In this section, we present some essential results on Bessel functions that are needed for the frequency-domain representation of MPI. We start with the definition of the Bessel function of first kind in series form.

Definition. *The Bessel function of first kind $J_n : \mathbb{R} \to \mathbb{R}$ with order $n \in \mathbb{Z}$ is defined as [13]*

$$J_n(\xi) = \sum_{m=0}^{\infty} \frac{(-1)^m}{m!\Gamma(m+n+1)} \left(\frac{\xi}{2}\right)^{2m+n}. \tag{29}$$

Lemma 4.9. *The inverse Fourier transform of the Bessel function of first kind $J_n(\omega_x)$ with order $n \in \mathbb{Z}$ is*

$$\mathscr{F}^{-1}[J_n(\omega_x)] = \begin{cases} \frac{\mathrm{i}^n T_{|n|}(x)}{\pi\sqrt{1-x^2}} & \text{for } |x|<1 \\ 0 & \text{else,} \end{cases} \tag{30}$$

where $T_n(x)$ denotes the n-th Chebyshev polynomial of the first kind, which can be written with trigonometric functions as [13]

$$T_n(x) = \cos(n \arccos(x)), \qquad |x|<1. \tag{31}$$

The inverse Fourier transform of $\frac{J_n(\omega_x)}{\mathrm{i}\omega_x}$ with order $n \in \mathbb{Z}$ is

$$\mathscr{F}^{-1}\left[\frac{J_n(\omega_x)}{\mathrm{i}\omega_x}\right] = \frac{\mathrm{i}^n}{\pi} V_n(x) \tag{32}$$

with

$$V_n(x) = \begin{cases} \operatorname{rect}\left(\frac{x}{2}\right)\left(-\frac{U_{|n|-1}(x)\sqrt{1-x^2}}{|n|}\right) & \text{if } |n|>0 \\ \frac{\pi}{2}\operatorname{sgn}(x+1) - \operatorname{rect}\left(\frac{x}{2}\right)\arccos(x) & \text{if } n=0, \end{cases} \tag{33}$$

where $U_n(x)$ denotes the n-th Chebyshev polynomial of the second kind [13]:

$$U_n(x) = \frac{\sin((n+1)\cdot\arccos(x))}{\sqrt{1-x^2}}, \qquad |x|<1. \tag{34}$$

Moreover, $V_n(x)$ and $T_n(x)$ have the mutual relationship

$$\frac{d}{dx} V_n(x) = \operatorname{rect}\left(\frac{x}{2}\right)\frac{T_{|n|}(x)}{\sqrt{1-x^2}}. \tag{35}$$

Proof. A proof for (30) can be found in the literature [17]. To prove (35) for $n \geq 1$, we simply take the derivative $\frac{d}{dx}V_n(x)$ with $V_n(x)$ according to (33):

$$\begin{aligned} \frac{d}{dx} V_n(x) &= -\frac{d}{dx}\frac{\sin(n\cdot\arccos(x))}{n} \\ &= \frac{\cos(n\arccos(x))}{\sqrt{1-x^2}}. \end{aligned}$$

A comparison with (31) confirms (35) for $n \geq 1$. For $n=0$ we have

$$V_0(x) = \frac{\pi}{2} - \arccos(x) = \arcsin(x), \qquad |x|<1.$$

Taking the derivative then results in

$$\frac{d}{dx} V_0(x) = \frac{1}{\sqrt{1-x^2}} = \frac{T_0(x)}{\sqrt{1-x^2}},$$

which confirms (35) for $n=0$. Moreover, for $|x|>1$ it is easy to verify that $\frac{d}{dx}V_n(x)=0$.

It remains to show that (32) holds. Based on the Fourier correspondence in (30) and the property $J_n(0)=0$, the Fourier integration theorem

$$\int_{-\infty}^{x} f(\tau)\,d\tau \longleftrightarrow \frac{1}{\mathrm{i}\omega} F(\omega) \quad \text{if} \quad F(0)=0$$

yields

$$\frac{\mathrm{i}^n}{\pi}\int_{-\infty}^{x} \operatorname{rect}\left(\frac{y}{2}\right)\frac{T_{|n|}(y)}{\sqrt{1-y^2}}\,dy \longleftrightarrow \frac{1}{\mathrm{i}\omega_x} J_n(\omega_x).$$

Fortunately, we only have to show that

$$g(x) := \frac{\mathrm{i}^n}{\pi}\int_{-\infty}^{x} \operatorname{rect}\left(\frac{y}{2}\right)\frac{T_{|n|}(y)}{\sqrt{1-y^2}}\,dy \overset{!}{=} \frac{\mathrm{i}^n}{\pi} V_n(x).$$

For $x \in [0,1]$ we obtain

$$g(x) = \frac{\mathrm{i}^n}{\pi} V_n(y)\Big|_{-1}^{x} = \frac{\mathrm{i}^n}{\pi}\left(V_n(x) - \underbrace{V_n(-1)}_{=0}\right) = \frac{\mathrm{i}^n}{\pi} V_n(x).$$

For $x<-1$ it holds that $g(x)=0$. For $x>1$, we have

$$\begin{aligned} g(x) &= \frac{\mathrm{i}^n}{\pi}\int_{-\infty}^{x} \operatorname{rect}\left(\frac{x}{2}\right)\frac{T_n(x)}{\sqrt{1-x^2}}\,dx \\ &= \left[\int_{-\infty}^{\infty} \operatorname{rect}\left(\frac{x}{2}\right)\frac{T_n(x)}{\sqrt{1-x^2}} \mathrm{e}^{\mathrm{i}\omega_x x}\,dx\right]_{\omega_x=0} \\ &= J_n(0) = 0. \end{aligned}$$

Overall, for $n \geq 1$ this validates that $g(x) = \frac{\mathrm{i}^n}{\pi} V_n(x)$. The case $n=0$ is more involved and will be treated separately in Lemmas 4.12 and 4.13. □

Corollary 4.10. *The function $\frac{J_n(\omega_x)}{\omega_x}$ is in $L^1(\mathbb{R}) \cap L^\infty(\mathbb{R})$, and the L^∞-norm has an upper bound of*

$$\left\| \frac{J_n(\omega_x)}{\omega_x} \right\|_{L^\infty} \leq C \frac{1}{n^{\frac{4}{3}}} \tag{36}$$

with a constant $C>0$ and $n>0$.

Proof. The upper bound on the L^∞-norm is shown in [18]. Thus, it remains to prove that $\frac{J_n(\omega_x)}{\omega_x} \in L^1(\mathbb{R})$. According to [19] we have

$$|J_n(\omega_x)| \leq \min(1, b\,n^{-\frac{1}{3}}, c\,|\omega_x|^{-\frac{1}{3}})$$

with constants $b = 0.674885\ldots$ and $c = 0.7857468704\ldots$. Observing that the function can be upper bounded by

$$\left|\frac{J_n(\omega_x)}{\omega_x}\right| \leq \operatorname{rect}\left(\frac{\omega_x}{2}\right) + \left(1 - \operatorname{rect}\left(\frac{\omega_x}{2}\right)\right)\frac{1}{|\omega_x|^{\frac{4}{3}}}$$

it holds that

$$\begin{aligned} \int_{-\infty}^{\infty}\left|\frac{J_n(\omega_x)}{\omega_x}\right| d\omega_x &\leq 2 + 2\int_{1}^{\infty}\frac{1}{|\omega_x|^{\frac{4}{3}}}\,d\omega_x \\ &= 2 - \frac{2}{(\frac{4}{3}-1)|\omega_x|^{\frac{4}{3}-1}}\Big|_{1}^{\infty} = 8 < \infty. \end{aligned}$$

□

IV.III. Product of Bessel function and Fourier transformed Langevin function

In this section a central result for the product of the Fourier transformed Langevin function with a Bessel function of first kind is given.

Lemma 4.11. *The function*

$$l_\nu^{3D}(\boldsymbol{\omega_x}) = J_\ell(\alpha_1\omega_{x_1})J_m(\alpha_2\omega_{x_2})J_n(\alpha_3\omega_{x_3})\hat{\mathscr{L}}_\nu(\boldsymbol{\omega_x}), \quad (37)$$

where $\hat{\mathscr{L}}_\nu(\boldsymbol{\omega_x})$ denotes the components of $\hat{\mathscr{L}}:\mathbb{R}^3\to\mathbb{C}^3$ and $J_\ell(\alpha_1\omega_{x_1})$, $J_m(\alpha_2\omega_{x_2})$, $J_n(\alpha_3\omega_{x_3})$ are Bessel functions of first kind with at least one $\alpha_i\neq 0$, is in $L^1(\mathbb{R}^3)$ if $|\ell|+|m|+|n|\geq 1$. An upper bound for the L^1-norm is given by

$$\|l_\nu^{3D}\|_{L^1} \leq \frac{C}{(\max(1,|\ell|)\max(1,|m|)\max(1,|n|))^{\frac{4}{3}}} \quad (38)$$

with $C>0$. Similarly, the bounds for the L^1-norms of

$$l_\nu^{2D}(\boldsymbol{\omega_x}) = J_\ell(\alpha_1\omega_{x_1})J_m(\alpha_2\omega_{x_2})\hat{\mathscr{L}}_\nu(\boldsymbol{\omega_x}) = \left[l_\nu^{3D}(\boldsymbol{\omega_x})\right]_{\substack{\alpha_3=0\\ n=0}} \quad (39)$$

and

$$l_\nu^{1D}(\boldsymbol{\omega_x}) = J_\ell(\alpha_1\omega_{x_1})\hat{\mathscr{L}}_\nu(\boldsymbol{\omega_x}) = \left[l_\nu^{3D}(\boldsymbol{\omega_x})\right]_{\substack{\alpha_2=\alpha_3=0\\ n=m=0}} \quad (40)$$

are given by (38) with the appropriate choice of n,m.

Proof. We consider the function $l_\nu^{3D}(\boldsymbol{\omega_x})$ from (37). Firstly, we consider the case where $|\ell|\geq 1$ and $n=m=0$ and define

$$f(\boldsymbol{\omega_x}) := \frac{J_\ell(\alpha_1\omega_{x_1})}{\omega_{x_1}} J_m(\alpha_2\omega_{x_2})J_n(\alpha_3\omega_{x_3})$$
$$g(\boldsymbol{\omega_x}) := \omega_{x_1}\hat{\mathscr{L}}_\nu(\boldsymbol{\omega_x}).$$

Using Lemma 4.8, the norm of $\|g\|_{L^1}$ is bounded by a constant c_1 with $0<c_1<\infty$. From Corollary 4.10 and using $\|J_0\|_\infty = 1$ we know that $\|f\|_{L^\infty}\leq C_1/|\ell|^{\frac{4}{3}}$. The Hölder inequality then yields

$$\|l_\nu^{3D}\|_{L^1} = \|f\cdot g\|_{L^1} \leq \|f\|_{L^\infty}\|g\|_{L^1} \leq \frac{C_1}{|\ell|^{\frac{4}{3}}}c_1 < \infty. \quad (41)$$

Secondly, we consider that $|\ell|\geq 1$, $|m|\geq 1$ and $n=0$. Now, we can split the function $l_\nu^{3D}(\boldsymbol{\omega_x}) = f(\boldsymbol{\omega_x})g(\boldsymbol{\omega_x})$ into

$$f(\boldsymbol{\omega_x}) := \frac{J_\ell(\alpha_1\omega_{x_1})}{\omega_{x_1}}\frac{J_m(\alpha_2\omega_{x_2})}{\omega_{x_2}} J_n(\alpha_3\omega_{x_3}),$$
$$g(\boldsymbol{\omega_x}) := \omega_{x_1}\omega_{x_2}\hat{\mathscr{L}}_\nu(\boldsymbol{\omega_x}).$$

Using Lemma 4.8, Corollary 4.10, and $\|J_0\|_\infty = 1$ the Hölder inequality then yields

$$\|l_\nu^{3D}\|_{L^1} = \|f\cdot g\|_{L^1} \leq \|f\|_{L^\infty}\|g\|_{L^1} \leq \frac{C_2}{|\ell|^{\frac{4}{3}}|m|^{\frac{4}{3}}}c_2 < \infty. \quad (42)$$

Next, we assume that $|\ell|$, $|m|$, and $|n|$ are larger than zero. In this case we can split $l_\nu^{3D}(\boldsymbol{\omega_x}) = f(\boldsymbol{\omega_x})g(\boldsymbol{\omega_x})$ into

$$f(\boldsymbol{\omega_x}) := \frac{J_\ell(\alpha_1\omega_{x_1})}{\omega_{x_1}}\frac{J_m(\alpha_2\omega_{x_2})}{\omega_{x_2}}\frac{J_n(\alpha_3\omega_{x_3})}{\omega_{x_3}},$$
$$g(\boldsymbol{\omega_x}) := \omega_{x_1}\omega_{x_2}\omega_{x_3}\hat{\mathscr{L}}_\nu(\boldsymbol{\omega_x}).$$

Now, using Lemma 4.8 and Corollary 4.10 the Hölder inequality yields

$$\|l_\nu^{3D}\|_{L^1} = \|f\cdot g\|_{L^1} \leq \|f\|_{L^\infty}\|g\|_{L^1} \leq \frac{C_3}{|\ell|^{\frac{4}{3}}|m|^{\frac{4}{3}}|n|^{\frac{4}{3}}}c_3 < \infty. \quad (43)$$

Expressions similar to (41), (42), and (43) can be derived for the other possible combinations of general $\ell,n,m\in\mathbb{Z}$ with $|\ell|+|m|+|n|\geq 1$. Altogether, these confirm (38) for all $\ell,m,n\in\mathbb{Z}$. □

Lemma 4.11 makes it possible to define the inverse Fourier Transform of products of $\hat{\mathscr{L}}_\nu(\boldsymbol{\omega_x})$ and Bessel functions of first kind, but first we state a Lemma that helps us to unify the notation.

Lemma 4.12. *The convolution of a function $F(x)\in L^\infty(\mathbb{R})$ that has the property $\lim_{x\to\pm\infty}F(x)=\pm c$ and $c\in\mathbb{R}$ with a scaled version of the function*

$$v_0(x) = \tfrac{d}{dx}V_0(x),$$

where $V_0(x)$ is defined in (33), yields

$$\begin{aligned}\int_{-\infty}^{\infty} F(x-y)\frac{1}{|\alpha|}v_0\left(\frac{y}{\alpha}\right)dy \\ = \int_{-\infty}^{\infty} f(x-y)\frac{\alpha}{|\alpha|}V_0\left(\frac{y}{\alpha}\right)dy, \quad \alpha\neq 0\end{aligned} \quad (44)$$

with $f(x) = \frac{d}{dx}F(x)$.

The proof of this Lemma is deferred to Appendix C.

We now consider the inverse Fourier Transform of products of $\hat{\mathscr{L}}_\nu(\boldsymbol{\omega_x})$ and Bessel functions of first kind.

Lemma 4.13. *The inverse Fourier transforms of products*

$$\hat{a}_\nu^{1D}(\boldsymbol{\omega_x}) := \frac{J_n(\alpha_1\omega_{x_1})e^{-i\omega_{x_2}c_2}e^{-i\omega_{x_3}c_3}\hat{\mathscr{L}}_\nu\left(\frac{\boldsymbol{G}^{-T}\boldsymbol{\omega_x}}{\beta}\right)}{\left|\det(\beta\boldsymbol{G})\right|}$$
$$\hat{a}_\nu^{2D}(\boldsymbol{\omega_x}) := \frac{J_n(\alpha_1\omega_{x_1})J_m(\alpha_2\omega_{x_2})e^{-i\omega_{x_3}c_3}\hat{\mathscr{L}}_\nu\left(\frac{\boldsymbol{G}^{-T}\boldsymbol{\omega_x}}{\beta}\right)}{\left|\det(\beta\boldsymbol{G})\right|}$$
$$\hat{a}_\nu^{3D}(\boldsymbol{\omega_x}) := \frac{J_n(\alpha_1\omega_{x_1})J_m(\alpha_2\omega_{x_2})J_\ell(\alpha_3\omega_{x_3})\hat{\mathscr{L}}_\nu\left(\frac{\boldsymbol{G}^{-T}\boldsymbol{\omega_x}}{\beta}\right)}{\left|\det(\beta\boldsymbol{G})\right|}, \quad (45)$$

of $\hat{\mathscr{L}}_\nu:\mathbb{R}^3\to\mathbb{C}$ with the Bessel functions of first kind $J_n(\alpha_1\omega_{x_1})$, $J_m(\alpha_2\omega_{x_2})$, and $J_\ell(\alpha_3\omega_{x_3})$ with $\alpha_i\neq 0$, $c_2,c_3\in$

$\mathbb{R}$ *and* $|n|+|m|+|\ell|\geq 1$ *are given by*

$$\mathscr{F}^{-1}\left[\hat{a}_\nu^{1\mathrm{D}}(\boldsymbol{\omega}_{\boldsymbol{x}})\right]=\frac{\mathrm{i}^n}{\pi\,\mathrm{sgn}(\alpha_1)}\int_{\mathbb{R}}\left[\frac{\partial}{\partial z_1}\mathscr{L}_\nu\left(\beta\boldsymbol{G}\begin{pmatrix}z_1\\x_2-c_2\\x_3-c_3\end{pmatrix}\right)\right]_{z_1=x_1-u_1}\cdot V_n\left(\frac{u_1}{\alpha_1}\right)du_1, \tag{46}$$

$$\mathscr{F}^{-1}\left[\hat{a}_\nu^{2\mathrm{D}}(\boldsymbol{\omega}_{\boldsymbol{x}})\right]=\frac{\mathrm{i}^{n+m}}{\pi^2\,\mathrm{sgn}(\alpha_1\alpha_2)}\int_{\mathbb{R}^2}\left[\frac{\partial^2}{\partial z_1\partial z_2}\mathscr{L}_\nu\left(\beta\boldsymbol{G}\begin{pmatrix}z_1\\z_2\\x_3-c_3\end{pmatrix}\right)\right]_{\substack{z_1=x_1-u_1\\z_2=x_2-u_2}}\cdot V_n\left(\frac{u_1}{\alpha_1}\right)V_m\left(\frac{u_2}{\alpha_2}\right)du_1\,du_2, \tag{47}$$

and

$$\mathscr{F}^{-1}\left[\hat{a}_\nu^{3\mathrm{D}}(\boldsymbol{\omega}_{\boldsymbol{x}})\right]=\frac{\mathrm{i}^{n+m+\ell}}{\pi^3\,\mathrm{sgn}(\alpha_1\alpha_2\alpha_3)}\int_{\mathbb{R}^3}\left[\frac{\partial^3}{\partial z_1\partial z_2\partial z_3}\mathscr{L}_\nu(\beta\boldsymbol{G}\boldsymbol{z})\right]_{\boldsymbol{z}=\boldsymbol{x}-\boldsymbol{u}}\cdot V_n\left(\frac{u_1}{\alpha_1}\right)V_m\left(\frac{u_2}{\alpha_2}\right)V_\ell\left(\frac{u_3}{\alpha_3}\right)d\boldsymbol{u}, \tag{48}$$

respectively.

Proof. According to Lemma 4.9 with $|n|\geq 1$ and the scaling theorem of the Fourier transform with $\alpha\neq 0$ we know that

$$\mathscr{F}^{-1}\left[\frac{J_n(\alpha\omega_x)}{\mathrm{i}\omega_x}\right]=\frac{\mathrm{i}^n}{\pi\,\mathrm{sgn}(\alpha)}V_n\left(\frac{x}{\alpha}\right),$$

$$\mathscr{F}^{-1}\left[\frac{\mathrm{i}\omega_{x_1}\hat{\mathscr{L}}_\nu\left(\frac{\boldsymbol{G}^{-T}\boldsymbol{\omega}_{\boldsymbol{x}}}{\beta}\right)}{\left|\det(\beta\boldsymbol{G})\right|}\right]=\frac{\partial}{\partial x_1}\left[\mathscr{L}_\nu(\beta\boldsymbol{G}\boldsymbol{x})\right],$$

$$\mathscr{F}^{-1}\left[\frac{\mathrm{i}\omega_{x_1}\mathrm{i}\omega_{x_2}\hat{\mathscr{L}}_\nu\left(\frac{\boldsymbol{G}^{-T}\boldsymbol{\omega}_{\boldsymbol{x}}}{\beta}\right)}{\left|\det(\beta\boldsymbol{G})\right|}\right]=\frac{\partial^2}{\partial x_1\partial x_2}\left[\mathscr{L}_\nu(\beta\boldsymbol{G}\boldsymbol{x})\right],$$

$$\mathscr{F}^{-1}\left[\frac{\mathrm{i}^3\omega_{x_1}\omega_{x_2}\omega_{x_3}\hat{\mathscr{L}}_\nu\left(\frac{\boldsymbol{G}^{-T}\boldsymbol{\omega}_{\boldsymbol{x}}}{\beta}\right)}{\left|\det(\beta\boldsymbol{G})\right|}\right]=\frac{\partial^3}{\partial x_1\partial x_2\partial x_3}\left[\mathscr{L}_\nu(\beta\boldsymbol{G}\boldsymbol{x})\right].$$

Moreover, we have the well-known relationship

$$\mathscr{F}^{-1}\left[\mathrm{e}^{-\mathrm{i}\omega_x c}\right]=\delta_0(x-c)$$

with $\delta_0(x)$ being the Dirac delta distribution. Now, using that a multiplication in Fourier domain is equivalent to a convolution in spatial domain we get (term by term) the results for $a_\nu^{1\mathrm{D}}(\boldsymbol{x})=\mathscr{F}^{-1}[\hat{a}_\nu^{1\mathrm{D}}(\boldsymbol{\omega}_{\boldsymbol{x}})]$, $a_\nu^{2\mathrm{D}}(\boldsymbol{x})=\mathscr{F}^{-1}[\hat{a}_\nu^{2\mathrm{D}}(\boldsymbol{\omega}_{\boldsymbol{x}})]$, and $a_\nu^{3\mathrm{D}}(\boldsymbol{x})=\mathscr{F}^{-1}[\hat{a}_\nu^{3\mathrm{D}}(\boldsymbol{\omega}_{\boldsymbol{x}})]$. These convolutions generally occur in all three dimensions. However, for $a_\nu^{1\mathrm{D}}(\boldsymbol{x})$ and $a_\nu^{2\mathrm{D}}(\boldsymbol{x})$, they effectively reduce to one- and two-dimensional ones, respectively, because the convolutions with Dirac delta distributions along the unused dimensions just result in phase shifts.

In case that either n,m or ℓ is zero, we still have the Fourier correspondence

$$\mathscr{F}^{-1}\left[J_0\left(\alpha_j\omega_{x_j}\right)\right]=\frac{1}{\pi}\frac{1}{|\alpha_j|}\,\mathrm{rect}\left(\frac{x_j}{\alpha_j}\right)\frac{1}{\sqrt{1-\left(\frac{x_j}{\alpha_j}\right)^2}}=\frac{1}{\pi}\frac{1}{|\alpha_j|}v_0\left(\frac{x_j}{\alpha_j}\right)$$

with $v_0(x)=\frac{d}{dx}V(x)$ as defined by Lemma 4.9 and Lemma 4.12. For $|n||m|>0$ and $\ell=0$, we have the following inverse Fourier transform for $\hat{a}_\nu^{3\mathrm{D}}(\boldsymbol{\omega}_{\boldsymbol{x}})$:

$$a_\nu^{3\mathrm{D}}(\boldsymbol{x})=\frac{\mathrm{i}^{n+m}}{\pi^3\,\mathrm{sgn}(\alpha_1\alpha_2)}\int_{\mathbb{R}^3}\left[\frac{\partial^2}{\partial z_1\partial z_2}\mathscr{L}_\nu(\beta\boldsymbol{G}\boldsymbol{z})\right]_{\boldsymbol{z}=\boldsymbol{x}-\boldsymbol{u}}\cdot V_n\left(\frac{u_1}{\alpha_1}\right)V_m\left(\frac{u_2}{\alpha_2}\right)\frac{1}{|\alpha_3|}v_0\left(\frac{u_3}{\alpha_3}\right)d\boldsymbol{u}.$$

Due to Lemma 4.8 we know that $\omega_{x_1}\omega_{x_2}\hat{\mathscr{L}}_\nu\left(\frac{\boldsymbol{G}^{-T}\boldsymbol{\omega}_{\boldsymbol{x}}}{\beta}\right)$ is in $L^1(\mathbb{R}^3)$. Therefore, the function $\frac{\partial^2}{\partial x_1\partial x_2}\left[\mathscr{L}_\nu(\beta\boldsymbol{G}\boldsymbol{x})\right]$ vanishes as its argument goes to plus or minus infinity and, thus, it is in $L^\infty(\mathbb{R}^3)$. This allows us to use Lemma 4.12, resulting in

$$a_\nu^{3\mathrm{D}}(\boldsymbol{x})=\frac{\mathrm{i}^{n+m}}{\pi^3\,\mathrm{sgn}(\alpha_1\alpha_2\alpha_3)}\int_{\mathbb{R}^3}\left[\frac{\partial^3}{\partial z_1\partial z_2\partial z_3}\mathscr{L}_\nu(\beta\boldsymbol{G}\boldsymbol{z})\right]_{\boldsymbol{z}=\boldsymbol{x}-\boldsymbol{u}}\cdot V_n\left(\frac{u_1}{\alpha_1}\right)V_m\left(\frac{u_2}{\alpha_2}\right)V_0\left(\frac{u_3}{\alpha_3}\right)d\boldsymbol{u}.$$

The expressions for $a^{3\mathrm{D}}(\boldsymbol{x})$ and $a^{2\mathrm{D}}(\boldsymbol{x})$ with other possible combinations of $|m|+|n|+|\ell|\geq 1$ follow likewise. For $a^{1\mathrm{D}}(\boldsymbol{x})$ the case $n=0$ is not needed. □

V. Fourier representation for a one-dimensional trajectory

For a one-dimensional excitation with a three-dimensional SPIO distribution, a closed-form representation of the temporal Fourier series coefficients has been derived in [2]. This commonly known result can also be deduced from Theorem 3.1 in the article. In addition to the known relationships, we will introduce a

spatial Fourier transform version $\hat{\boldsymbol{s}}_k(\boldsymbol{\omega_x})$ of $\boldsymbol{s}_k(\boldsymbol{x})$ in the following.

Definition. *Let f_x be an arbitrary excitation frequency of our MPI scanner. The drive field along the x-axis then has the form*

$$\boldsymbol{H}^D(t) = \begin{pmatrix} -A_x \sin(\omega_x t + \varphi_x) \\ -c_y \\ -c_z \end{pmatrix}, \tag{49}$$

where $\omega_x = 2\pi f_x$ denotes the angular frequency, A_x is the amplitude, $\varphi_x \in [0, 2\pi)$ is a phase offset and $c_y, c_z \in \mathbb{R}$ are time independent drive-field offsets. The homogeneous selection field $\boldsymbol{H}^S(\boldsymbol{x}) = \boldsymbol{G}\boldsymbol{x}$ of the MPI scanner is, without loss of generality, assumed to be diagonal:

$$\boldsymbol{G} = \begin{pmatrix} G_x & 0 & 0 \\ 0 & G_y & 0 \\ 0 & 0 & G_z \end{pmatrix}. \tag{50}$$

According to the Maxwell equations the magnetic field fulfills $G_x + G_y + G_z = 0$.

The position of the FFP is given by [1, 11, 20]

$$\boldsymbol{x}_{\mathrm{FFP}}(t) = -\boldsymbol{G}^{-1}\boldsymbol{H}^D(t) \tag{51}$$

and has the period length $T_D = \frac{1}{f_x}$ and, consequently, $f_D = f_x$. With this information we can now formulate the Fourier representation for MPI with a one-dimensional trajectory in a theorem.

Theorem 5.1. *The Fourier series coefficients $\boldsymbol{s}_k : \mathbb{R}^3 \to \mathbb{C}^3$ of the MPI system function for a one-dimensional FFP-trajectory and $k \in \mathbb{Z}\backslash\{0\}$ can be expressed in terms of products of $V_\ell : \mathbb{R} \to \mathbb{R}$ convolved along the spatial dimensions with the spatial derivative of the Langevin function $\mathscr{L} : \mathbb{R}^3 \to \mathbb{R}^3$ by*

$$\boldsymbol{s}_k(\boldsymbol{x}) = \frac{(-\mathrm{i})^{k+1}\omega_k \mathrm{e}^{\mathrm{i}\varphi_x k}}{\pi} \frac{\operatorname{sgn}(A_x)}{\operatorname{sgn}(G_x)} \int_{\mathbb{R}} \left[\frac{\partial}{\partial z_1} \mathscr{L}\left(\beta \boldsymbol{G} \begin{pmatrix} z_1 \\ x_2 - \frac{c_y}{G_y} \\ x_3 - \frac{c_z}{G_z} \end{pmatrix} \right) \right]_{z_1 = x_1 - u_1} V_k\left(\frac{G_x}{A_x} u_1\right) du_1, \tag{52}$$

with

$$V_n(x) = \operatorname{rect}\left(\frac{x}{2}\right) \left(-\frac{U_{|n|-1}(x)\sqrt{1-x^2}}{|n|} \right), \qquad |n| > 0 \tag{53}$$

and $U_{n-1}(x)$ being the Chebyshev polynomial of second kind and order $n-1$.

Equivalently, the spatial Fourier domain representation of $\boldsymbol{s}_k(\boldsymbol{x})$ is given by

$$\hat{\boldsymbol{s}}_k(\boldsymbol{\omega_x}) = \frac{(-1)^{k+1}\mathrm{i}\omega_k \mathrm{e}^{\mathrm{i}\varphi_x k}}{\left|\det(\beta \boldsymbol{G})\right|} \hat{\mathscr{L}}\left(\frac{\boldsymbol{G}^{-T}\boldsymbol{\omega_x}}{\beta} \right) \cdot J_k\left(\omega_{x_1} \frac{A_x}{G_x}\right) \mathrm{e}^{-\mathrm{i}\frac{c_y}{G_y}\omega_{x_2}} \mathrm{e}^{-\mathrm{i}\frac{c_z}{G_z}\omega_{x_3}}, \tag{54}$$

where $J_n(\omega_x)$ denotes the n-th Bessel function of first kind and $\hat{\mathscr{L}} : \mathbb{R}^3 \to \mathbb{C}^3$ reads

$$\hat{\mathscr{L}}(\boldsymbol{\omega_x}) = -4\pi^2 \mathrm{i} \frac{(\pi\|\boldsymbol{\omega_x}\| + 1)\mathrm{e}^{\pi\|\boldsymbol{\omega_x}\|} - 1}{\|\boldsymbol{\omega_x}\|^2 (\mathrm{e}^{\pi\|\boldsymbol{\omega_x}\|} - 1)^2} \frac{\boldsymbol{\omega_x}}{\|\boldsymbol{\omega_x}\|}. \tag{55}$$

For $k = 0$ it holds that $\boldsymbol{s}_0(\boldsymbol{x}) = \boldsymbol{0}$ and $\hat{\boldsymbol{s}}_0(\boldsymbol{\omega_x}) = \boldsymbol{0}$.

Note that the expression for $\boldsymbol{s}_k(\boldsymbol{x})$ in (52) is the same as in [2] when the phase offset is set to $\varphi_x = \frac{\pi}{2}$ and we use $c_y = c_z = 0$.

Proof of Theorem 5.1. Firstly, observe that

$$\boldsymbol{x}_{\mathrm{FFP}}\left(\frac{z}{2\pi f_D}\right) = \begin{pmatrix} \frac{A_x}{G_x}\sin(z + \varphi_x) \\ \frac{c_y}{G_y} \\ \frac{c_z}{G_z} \end{pmatrix}.$$

To compute the mapping function $P(\boldsymbol{\omega_x}, k)$ defined in (11),

$$P(\boldsymbol{\omega_x}, k) = \frac{1}{2\pi} \int_{-\pi}^{\pi} \mathrm{e}^{\mathrm{i}\boldsymbol{\omega_x}^T \boldsymbol{x}_{\mathrm{FFP}}\left(\frac{z}{2\pi f_D}\right)} \mathrm{e}^{-\mathrm{i}kz}\, dz \tag{56}$$

we rewrite the term $\mathrm{e}^{\mathrm{i}\boldsymbol{\omega_x}^T \boldsymbol{x}_{\mathrm{FFP}}\left(\frac{z}{2\pi f_D}\right)}$ as

$$\mathrm{e}^{\mathrm{i}\boldsymbol{\omega_x}^T \boldsymbol{x}_{\mathrm{FFP}}\left(\frac{z}{2\pi f_D}\right)} = \mathrm{e}^{\mathrm{i}\omega_{x_1}\frac{A_x}{G_x}\sin(z+\varphi_x)} \mathrm{e}^{\mathrm{i}\frac{c_y}{G_y}\omega_{x_2}} \mathrm{e}^{\mathrm{i}\frac{c_z}{G_z}\omega_{x_3}}$$

and by using the Jacobi-Anger expansion [21]

$$\mathrm{e}^{\mathrm{i}z\sin(\theta)} = \sum_{n=-\infty}^{\infty} J_n(z)\mathrm{e}^{\mathrm{i}n\theta},$$

as

$$\mathrm{e}^{\mathrm{i}\boldsymbol{\omega_x}^T \boldsymbol{x}_{\mathrm{FFP}}\left(\frac{z}{2\pi f_D}\right)} = \sum_{n=-\infty}^{\infty} J_n\left(\omega_{x_1}\frac{A_x}{G_x}\right) \mathrm{e}^{\mathrm{i}n(z+\varphi_x)} \mathrm{e}^{\mathrm{i}\frac{c_y}{G_y}\omega_{x_2}} \mathrm{e}^{\mathrm{i}\frac{c_z}{G_z}\omega_{x_3}}. \tag{57}$$

Inserting (57) into (56), reordering the terms, and carrying out the integration yields

$$\begin{aligned} P(\boldsymbol{\omega_x}, k) &= \sum_{n=-\infty}^{\infty} \mathrm{e}^{\mathrm{i}\varphi_x n} J_n\left(\omega_{x_1}\frac{A_x}{G_x}\right) \mathrm{e}^{\mathrm{i}\frac{c_y}{G_y}\omega_{x_2}} \mathrm{e}^{\mathrm{i}\frac{c_z}{G_z}\omega_{x_3}} \\ &\quad \cdot \underbrace{\frac{1}{2\pi}\int_{-\pi}^{\pi} \mathrm{e}^{\mathrm{i}(n-k)z}\, dz}_{=\delta_{(n,k)}} \\ &= \mathrm{e}^{\mathrm{i}\varphi_x k} J_k\left(\omega_{x_1}\frac{A_x}{G_x}\right) \mathrm{e}^{\mathrm{i}\frac{c_y}{G_y}\omega_{x_2}} \mathrm{e}^{\mathrm{i}\frac{c_z}{G_z}\omega_{x_3}}, \end{aligned} \tag{58}$$

where

$$\delta_{(n,k)} = \begin{cases} 1 & \text{if } k = n \\ 0 & \text{otherwise} \end{cases}$$

denotes the Kronecker delta.

We now consider $\boldsymbol{g}_k$ from (10) with $\hat{\boldsymbol{h}}(\boldsymbol{\omega_x})$ from (12):

$$\boldsymbol{g}_k = \frac{\mathrm{i}\omega_k}{(2\pi)^3} \int_{\mathbb{R}^3} \frac{\hat{c}(\boldsymbol{\omega_x})}{\left|\det(\beta \boldsymbol{G})\right|} \hat{\mathscr{L}}\left(\frac{\boldsymbol{G}^{-T}\boldsymbol{\omega_x}}{\beta}\right) P(\boldsymbol{\omega_x}, k)\, d\boldsymbol{\omega_x}. \tag{59}$$

Inserting $P(\boldsymbol{\omega}_x, k)$ from (58) into (59) and comparing the obtained expression with (54) under use of $\hat{\mathcal{L}}(-\boldsymbol{\omega}_x) = -\hat{\mathcal{L}}(\boldsymbol{\omega}_x)$ and $J_k(-\omega) = (-1)^k J_k(\omega)$ yields

$$\begin{aligned} \boldsymbol{g}_k &= \frac{1}{(2\pi)^3} \int_{\mathbb{R}^3} \hat{c}(\boldsymbol{\omega}_x) \hat{\boldsymbol{s}}_k(-\boldsymbol{\omega}_x)\, d\boldsymbol{\omega}_x \\ &= \frac{1}{(2\pi)^3} \int_{\mathbb{R}^3} \hat{c}(-\boldsymbol{\omega}_x) \hat{\boldsymbol{s}}_k(\boldsymbol{\omega}_x)\, d\boldsymbol{\omega}_x. \end{aligned} \tag{60}$$

Now, by using that $c(\boldsymbol{x})$ is real-valued and that its Fourier transform has the conjugate symmetry $\hat{c}(-\boldsymbol{\omega}_x) = \hat{c}^*(\boldsymbol{\omega}_x)$, we can apply Parseval's theorem to obtain the original relationship (9):

$$\boldsymbol{g}_k = \int_{\mathbb{R}^3} c(\boldsymbol{x}) \boldsymbol{s}_k(\boldsymbol{x})\, d\boldsymbol{x}. \tag{61}$$

This proves that $\hat{\boldsymbol{s}}_k(\boldsymbol{\omega}_x)$ according to (54) is the spatial-frequency representation of $\boldsymbol{s}_k(\boldsymbol{x})$. Using Lemma 4.13 and observing that the expression in $\hat{a}_\nu^{\mathrm{1D}}(\boldsymbol{\omega}_x)$ is equivalent to (54) up to a factor, we get $\boldsymbol{s}_k(\boldsymbol{x})$ according to (52) as the inverse Fourier transform of (54), which was to be proven. □

VI. Fourier representation for two-dimensional Lissajous trajectories

Definition. *To define the trajectory, let $N_B \in \mathbb{N}$ be a frequency divider with $N_B \geq 2$ and f_B an arbitrary basis frequency of our MPI scanner. Then the excitation frequencies for the two-dimensional Lissajous FFP-trajectory are given by $f_x = \frac{f_B}{N_B}$ and $f_y = \frac{f_B}{N_B - 1}$. The corresponding angular frequencies are $\omega_x = 2\pi f_x$ and $\omega_y = 2\pi f_y$, respectively. The 2D drive field can be expressed as*

$$\boldsymbol{H}^D(t) = \begin{pmatrix} -A_x \sin(\omega_x t + \varphi_x) \\ -A_y \sin(\omega_y t + \varphi_y) \\ -c_z \end{pmatrix}, \tag{62}$$

where $A_x, A_y \in \mathbb{R}$ denote the drive-field amplitudes, $\varphi_x, \varphi_y \in [0, 2\pi)$ are the phase offsets, and $c_z \in \mathbb{R}$ is a time-independent drive-field offset in the third dimension. The homogeneous selection field $\boldsymbol{H}^S(\boldsymbol{x}) = \boldsymbol{G}\boldsymbol{x}$ of the MPI scanner has a gradient matrix $\boldsymbol{G} \in \mathbb{R}^{3\times 3}$ as in (50).

Similar to (51) the position of the FFP is given by

$$\boldsymbol{x}_{\mathrm{FFP}}(t) = -\boldsymbol{G}^{-1} \boldsymbol{H}^D(t), \tag{63}$$

where the trajectory is periodic with period length

$$T_D = \frac{1}{f_D} = \frac{N_B(N_B - 1)}{f_B}.$$

A direct expression for the series coefficients of the MPI system function is given in the following Theorem.

Theorem 6.1. *The Fourier series coefficients $\boldsymbol{s}_k : \mathbb{R}^3 \to \mathbb{C}^3$ of the MPI system function for a two-dimensional Lissajous FFP-trajectory with the phase offsets $\varphi_x = \varphi_y = 0$ and $k \in \mathbb{Z}\backslash\{0\}$ can be expressed in terms of tensor products of $V_\ell : \mathbb{R} \to \mathbb{R}$ convolved along each spatial dimension with the spatial derivative of the Langevin function $\mathcal{L} : \mathbb{R}^3 \to \mathbb{R}^3$ by*

$$\begin{aligned} \boldsymbol{s}_k(\boldsymbol{x}) = \sum_{\lambda \in \mathbb{Z}} \frac{(-\mathrm{i})^{\lambda+1} \omega_k}{\pi^2} \frac{\operatorname{sgn}(A_x A_y)}{\operatorname{sgn}(G_x G_y)} \\ \int_{\mathbb{R}^2} \left[\frac{\partial^2}{\partial z_1 \partial z_2} \mathcal{L}\left(\beta \boldsymbol{G} \begin{pmatrix} z_1 \\ z_2 \\ x_3 - \frac{c_z}{G_z} \end{pmatrix} \right) \right]_{\substack{z_1 = x_1 - u_1 \\ z_2 = x_2 - u_2}} \cdot \\ V_{-k+\lambda N_B}\left(\frac{G_x}{A_x} u_1 \right) V_{k-\lambda(N_B-1)}\left(\frac{G_y}{A_y} u_2 \right) du_1\, du_2, \end{aligned} \tag{64}$$

where

$$V_n(x) = \begin{cases} \operatorname{rect}\left(\frac{x}{2}\right)\left(-\frac{U_{|n|-1}(x)\sqrt{1-x^2}}{|n|} \right) & \text{if } |n| > 0 \\ \frac{\pi}{2} \operatorname{sgn}(x+1) - \operatorname{rect}\left(\frac{x}{2}\right) \arccos(x) & \text{if } n = 0 \end{cases} \tag{65}$$

and $U_{n-1}(x)$ denotes the Chebyshev polynomial of second kind and order $n-1$.

Equivalently, the spatial Fourier domain representation of $\boldsymbol{s}_k(\boldsymbol{x})$ can be expressed as

$$\begin{aligned} \hat{\boldsymbol{s}}_k(\boldsymbol{\omega}_x) = \sum_{\lambda=-\infty}^{\infty} \frac{(-1)^{\lambda+1} \mathrm{i}\omega_k}{|\det(\beta \boldsymbol{G})|} \hat{\mathcal{L}}\left(\frac{\boldsymbol{G}^{-T} \boldsymbol{\omega}_x}{\beta} \right) \mathrm{e}^{-\mathrm{i}\omega_{x_3} \frac{c_z}{G_z}} \cdot \\ J_{-k+\lambda N_B}\left(\omega_{x_1} \frac{A_x}{G_x} \right) J_{k-\lambda(N_B-1)}\left(\omega_{x_2} \frac{A_y}{G_y} \right), \end{aligned} \tag{66}$$

where $J_n(x)$ denotes the n-th Bessel function of first kind and $\hat{\mathcal{L}} : \mathbb{R}^3 \to \mathbb{C}^3$ is given by

$$\hat{\mathcal{L}}(\boldsymbol{\omega}_x) = -4\pi^2 \mathrm{i} \frac{(\pi \|\boldsymbol{\omega}_x\| + 1)\mathrm{e}^{\pi\|\boldsymbol{\omega}_x\|} - 1}{\|\boldsymbol{\omega}_x\|^2 (\mathrm{e}^{\pi\|\boldsymbol{\omega}_x\|} - 1)^2} \frac{\boldsymbol{\omega}_x}{\|\boldsymbol{\omega}_x\|}. \tag{67}$$

For $k = 0$ it holds that $\boldsymbol{s}_0(\boldsymbol{x}) = \boldsymbol{0}$ and $\hat{\boldsymbol{s}}_0(\boldsymbol{\omega}_x) = \boldsymbol{0}$.

We give the proof of this theorem in several steps. First, we derive an expression for the mapping function $P(\boldsymbol{\omega}_x, k)$ introduced in (11) for the special case of a two-dimensional FFP-Lissajous trajectory. The result is given in the following Lemma.

Lemma 6.2. *The mapping function $P : \mathbb{R}^3 \times \mathbb{Z} \to \mathbb{C}$ for the two-dimensional FFP-Lissajous trajectory $\boldsymbol{x}_{\mathrm{FFP}} : \mathbb{R} \to \mathbb{R}^3$ in Theorem 3.1 is given by*

$$\begin{aligned} P(\boldsymbol{\omega}_x, k) = \sum_{n,\ell \in \mathbb{Z}} \Bigg[\mathrm{e}^{\mathrm{i}(n\varphi_x + \ell\varphi_y)} J_n\left(\omega_{x_1} \frac{A_x}{G_x} \right) J_\ell\left(\omega_{x_2} \frac{A_y}{G_y} \right) \\ \cdot \delta_{(n(N_B-1)+\ell N_B, k)} \Bigg] \mathrm{e}^{\mathrm{i}\omega_{x_3} \frac{c_z}{G_z}}. \end{aligned} \tag{68}$$

Proof. To confirm (68), we consider $P(\boldsymbol{\omega}_x, k)$ according to (11),

$$P(\boldsymbol{\omega}_x, k) = \frac{1}{2\pi} \int_{-\pi}^{\pi} \mathrm{e}^{\mathrm{i}\boldsymbol{\omega}_x^T \boldsymbol{x}_{\mathrm{FFP}}\left(\frac{z}{2\pi f_D}\right)} \mathrm{e}^{-\mathrm{i}kz}\, dz \tag{69}$$

and insert the particular Lissajous trajectory. For the position of the FFP it turns out that

$$\boldsymbol{x}_{\mathrm{FFP}}\left(\frac{z}{2\pi f_D}\right)=\begin{pmatrix}\frac{A_x}{G_x}\sin\left(\frac{f_x}{f_D}z+\varphi_x\right)\\ \frac{A_y}{G_y}\sin\left(\frac{f_y}{f_D}z+\varphi_y\right)\\ \frac{c_z}{G_z}\end{pmatrix}=\begin{pmatrix}\frac{A_x}{G_x}\sin\big((N_B-1)z+\varphi_x\big)\\ \frac{A_y}{G_y}\sin\big(N_Bz+\varphi_y\big)\\ \frac{c_z}{G_z}\end{pmatrix}.$$

Using the Jacobi-Anger expansion [21]

$$\mathrm{e}^{\mathrm{i}z\sin(\theta)}=\sum_{n=-\infty}^{\infty}J_n(z)\mathrm{e}^{\mathrm{i}n\theta},$$

we can reformulate the term to be integrated as

$$\begin{aligned}&\mathrm{e}^{\mathrm{i}\boldsymbol{\omega}_{\boldsymbol{x}}^T\boldsymbol{x}_{\mathrm{FFP}}\left(\frac{z}{2\pi f_D}\right)}\mathrm{e}^{-\mathrm{i}kz}\\&=\mathrm{e}^{\mathrm{i}\omega_{x_1}\frac{A_x}{G_x}\sin\left((N_B-1)z+\varphi_x\right)}\mathrm{e}^{\mathrm{i}\omega_{x_2}\frac{A_y}{G_y}\sin\left(N_Bz+\varphi_y\right)}\mathrm{e}^{\mathrm{i}\omega_{x_3}\frac{c_z}{G_z}}\mathrm{e}^{-\mathrm{i}kz}\\&=\left(\sum_{n=-\infty}^{\infty}\mathrm{e}^{\mathrm{i}n\varphi_x}J_n\left(\omega_{x_1}\frac{A_x}{G_x}\right)\mathrm{e}^{\mathrm{i}n(N_B-1)z}\right)\\&\quad\cdot\left(\sum_{\ell=-\infty}^{\infty}\mathrm{e}^{\mathrm{i}\ell\varphi_y}J_\ell\left(\omega_{x_2}\frac{A_y}{G_y}\right)\mathrm{e}^{\mathrm{i}\ell N_Bz}\right)\cdot\mathrm{e}^{\mathrm{i}\omega_{x_3}\frac{c_z}{G_z}}\mathrm{e}^{-\mathrm{i}kz}\\&=\sum_{n=-\infty}^{\infty}\sum_{\ell=-\infty}^{\infty}\Bigg[\mathrm{e}^{\mathrm{i}(n\varphi_x+\ell\varphi_y)}\\&\quad\cdot J_n\left(\omega_{x_1}\frac{A_x}{G_x}\right)J_\ell\left(\omega_{x_2}\frac{A_y}{G_y}\right)\mathrm{e}^{\mathrm{i}[n(N_B-1)+\ell N_B-k]z}\Bigg]\mathrm{e}^{\mathrm{i}\omega_{x_3}\frac{c_z}{G_z}}.\end{aligned}$$

With this, (69) yields

$$\begin{aligned}P(\boldsymbol{\omega}_{\boldsymbol{x}},k)&=\sum_{n,\ell\in\mathbb{Z}}\Bigg[\mathrm{e}^{\mathrm{i}(n\varphi_x+\ell\varphi_y)}J_n\left(\omega_{x_1}\frac{A_x}{G_x}\right)J_\ell\left(\omega_{x_2}\frac{A_y}{G_y}\right)\\&\qquad\cdot\frac{1}{2\pi}\int_{-\pi}^{\pi}\mathrm{e}^{\mathrm{i}[n(N_B-1)+\ell N_B-k]z}\,dz\Bigg]\mathrm{e}^{\mathrm{i}\omega_{x_3}\frac{c_z}{G_z}}\\&=\sum_{n,\ell\in\mathbb{Z}}\Bigg[\mathrm{e}^{\mathrm{i}(n\varphi_x+\ell\varphi_y)}J_n\left(\omega_{x_1}\frac{A_x}{G_x}\right)J_\ell\left(\omega_{x_2}\frac{A_y}{G_y}\right)\\&\qquad\cdot\delta_{(n(N_B-1)+\ell N_B,k)}\Bigg]\mathrm{e}^{\mathrm{i}\omega_{x_3}\frac{c_z}{G_z}}.\end{aligned}$$

In particular, for $\varphi_x=\varphi_y=0$, which should be chosen, we obtain

$$P(\boldsymbol{\omega}_{\boldsymbol{x}},k)=\left(\sum_{n,\ell\in\mathbb{Z}}J_n\left(\omega_{x_1}\frac{A_x}{G_x}\right)J_\ell\left(\omega_{x_2}\frac{A_y}{G_y}\right)\delta_{(n(N_B-1)+\ell N_B,k)}\right)\cdot\mathrm{e}^{\mathrm{i}\omega_{x_3}\frac{c_z}{G_z}}.$$

□

The next Lemma helps us to remove the double sum in the mapping function $P(\boldsymbol{\omega}_{\boldsymbol{x}},k)$.

Lemma 6.3. *The constraint*

$$n(N_B-1)+\ell N_B=k \tag{70}$$

with $n,\ell,k\in\mathbb{Z}$ is fulfilled for the following line equation

$$\begin{pmatrix}n\\ \ell\end{pmatrix}=\begin{pmatrix}-k\\ k\end{pmatrix}+\lambda\begin{pmatrix}N_B\\ 1-N_B\end{pmatrix}, \tag{71}$$

with $\lambda\in\mathbb{Z}$.

Proof. To prove the lemma, we insert (71) into (70). This yields

$$\begin{aligned}n(N_B-1)+\ell N_B&=(-k+\lambda N_B)(N_B-1)+(k-\lambda(N_B-1))N_B\\&=-k(N_B-1)+kN_B+\lambda N_B(N_B-1)\\&\quad-\lambda(N_B-1)N_B\\&=k.\end{aligned}$$

Assuming $N_B\geq 2$, $N_B\in\mathbb{N}$, we need to show that only $\lambda\in\mathbb{Z}$ guarantees that $n,\ell\in\mathbb{Z}$. For this, we consider $\lambda\in\mathbb{R}$ with $\lambda=\hat{\lambda}+\beta$, $\beta\in[0,1]$ such that $\hat{\lambda},n,\ell\in\mathbb{Z}$. Then the following two constraints have to hold

$$\begin{aligned}n&=-k+\hat{\lambda}N_B+\beta N_B\in\mathbb{Z},\ \text{and}\\ \ell&=k-\hat{\lambda}(N_B-1)-\beta(N_B-1)\in\mathbb{Z}.\end{aligned}$$

By adding up both constraint we get

$$n+\ell=\hat{\lambda}+\beta\in\mathbb{Z}.$$

For $n,\ell,\hat{\lambda}\in\mathbb{Z}$ only $\beta=0$ and $\beta=1$ are valid solutions, confirming that $\lambda\in\mathbb{Z}$. □

Based on Lemma 6.3 the expression for $P(\boldsymbol{\omega}_{\boldsymbol{x}},k)$ in Lemma 6.2 can be rewritten in a simplified form:

Corollary 6.4. *The mapping function $P:\mathbb{R}^3\times\mathbb{Z}\to\mathbb{C}$ for the two-dimensional FFP-Lissajous trajectory $\boldsymbol{x}_{\mathrm{FFP}}:\mathbb{R}\to\mathbb{R}^3$ is for $\varphi_x=\varphi_y=0$ simplified to*

$$P(\boldsymbol{\omega}_{\boldsymbol{x}},k)=\left(\sum_{\lambda=-\infty}^{\infty}J_{-k+\lambda N_B}\left(\omega_{x_1}\frac{A_x}{G_x}\right)J_{k-\lambda(N_B-1)}\left(\omega_{x_2}\frac{A_y}{G_y}\right)\right)\cdot\mathrm{e}^{\mathrm{i}\omega_{x_3}\frac{c_z}{G_z}}. \tag{72}$$

We now turn to the frequency representation of the 3D MPI system equation with two-dimensional excitation. With the same arguments as in the proof of Theorem 5.1 in (59), (60), (61) and additionally using $(-1)^{-k+\lambda N_B}(-1)^{k-\lambda(N_B-1)}=(-1)^{\lambda}$, the 3D system function in Fourier space is given by (66).

We now need to show that the components of $\hat{\boldsymbol{s}}_k(\boldsymbol{\omega}_{\boldsymbol{x}})$, denoted as $\hat{s}_{yk}(\boldsymbol{\omega}_{\boldsymbol{x}})$, are in $L^1(\mathbb{R}^3)$. For this, we make use of Lemma 4.11 and assume that $|k|>0$. The estimate in (38) is scale invariant with respect to $\boldsymbol{G}^{-T}$, β, $\frac{A_x}{G_x}$, $\frac{A_y}{G_y}$, and $\frac{A_z}{G_z}$ up to a constant factor. Additionally all factors can

be combined into constants $C_1 > 0$ and $C_2 > 0$. Using $\|e^{-i\omega_{x_3}\alpha_z}\|_{L^\infty} = 1$ it can be shown that

$$\begin{aligned}
&\|\hat{s}_{\nu k}\|_{L^1} \\
&\leq C_1 \sum_{\lambda\in\mathbb{Z}} \int_{\mathbb{R}^3} |\hat{\mathscr{L}}_\nu(\boldsymbol{\omega}_{\boldsymbol{x}}) J_{-k+\lambda N_B}(\omega_{x_1}) J_{k-\lambda(N_B-1)}(\omega_{x_2})| d\boldsymbol{\omega}_{\boldsymbol{x}} \\
&\leq C_2 \sum_{\lambda\in\mathbb{Z}} \frac{1}{\max(1,|k-\lambda N_B|^{\frac{4}{3}})\max(1,|k-\lambda(N_B-1)|^{\frac{4}{3}})} \\
&< \infty.
\end{aligned}$$

We used that for $|k| > 0$ there is no $\lambda \in \mathbb{Z}$ such that $-k + \lambda N_B = 0$ and $k - \lambda(N_B - 1) = 0$. For $k = 0$, by arguments that the measured voltage signal is zero mean, we may set $\boldsymbol{s}_0(\boldsymbol{x}) = \boldsymbol{0}$ and $\hat{\boldsymbol{s}}_0(\boldsymbol{\omega}_{\boldsymbol{x}}) = \boldsymbol{0}$. This shows that the series is well defined and that the system function $\hat{\boldsymbol{s}}_k(\boldsymbol{\omega}_{\boldsymbol{x}})$ is in $L^1(\mathbb{R}^3)$, which makes it possible to define the inverse Fourier transform.

Observing, that the terms in the series expansion (66) are similar to $\hat{a}_\nu^{2D}(\boldsymbol{\omega}_{\boldsymbol{x}})$ in Lemma 4.13 up to factors $(-1)^{\lambda+1} i\omega_k$ and using that the Fourier transform is a linear operator, we can perform the inverse Fourier transform of $\hat{\boldsymbol{s}}_k(\boldsymbol{\omega}_{\boldsymbol{x}})$ and calculate

$$\begin{aligned}
\boldsymbol{s}_k(\boldsymbol{x}) = \sum_{\lambda\in\mathbb{Z}} &\frac{(-i)^{\lambda+1}\omega_k}{\pi^2} \frac{\operatorname{sgn}(A_x A_y)}{\operatorname{sgn}(G_x G_y)} \\
&\cdot \int_{\mathbb{R}^2} \left[\frac{\partial^2}{\partial z_1 \partial z_2} \mathscr{L}\left(\beta \boldsymbol{G} \begin{pmatrix} z_1 \\ z_2 \\ x_3 - \frac{c_z}{G_z} \end{pmatrix} \right) \right]_{\substack{z_1 = x_1 - u_1 \\ z_2 = x_2 - u_2}} \\
&\cdot V_{-k+\lambda N_B}\left(\frac{G_x}{A_x} u_1\right) V_{k-\lambda(N_B-1)}\left(\frac{G_y}{A_y} u_2\right) du_1\, du_2.
\end{aligned}$$

This finally confirms (64), and the proof of Theorem 6.1 is finished. Note that, from a mathematical point of view, $c_z = 0$ is a useful choice.

VII. Fourier representation for three-dimensional Lissajous trajectories

We start with the definition of three-dimensional Lissajous FFP-trajectories:

Definition. *Let $N_B \in \mathbb{N}$ be a frequency divider with $N_B \geq 2$ and let f_B be an arbitrary basis frequency of our MPI scanner. Then the excitation frequencies are chosen in such a way that $f_x = \frac{f_B}{N_B}$, $f_y = \frac{f_B}{N_B - 1}$, and $f_z = \frac{f_B}{N_B + 1}$. The drive field then has the form*

$$\boldsymbol{H}^D(t) = \begin{pmatrix} -A_x \sin(\omega_x t + \varphi_x) \\ -A_y \sin(\omega_y t + \varphi_y) \\ -A_z \sin(\omega_z t + \varphi_z) \end{pmatrix}, \tag{73}$$

where $\omega_{x,y,z} = 2\pi f_{x,y,z}$ denote the angular frequencies, A_x, A_y, A_z are the amplitudes, and $\varphi_x, \varphi_y, \varphi_z$ are the phase shifts. The homogeneous selection field $\boldsymbol{H}^S(\boldsymbol{x}) = \boldsymbol{G}\boldsymbol{x}$ of the MPI scanner has a gradient matrix $\boldsymbol{G} \in \mathbb{R}^{3\times 3}$ as in (50).

Similar to (51) and (63), the position of the FFP is given by

$$\boldsymbol{x}_{\mathrm{FFP}}(t) = -\boldsymbol{G}^{-1}\boldsymbol{H}^D(t),$$

where the position of the FFP $\boldsymbol{x}_{\mathrm{FFP}}(t)$ now has the period length

$$T_D = \begin{cases} \dfrac{(N_B+1)N_B(N_B-1)}{f_B} & \text{for } N_B \text{ even} \\ \dfrac{(N_B+1)N_B(N_B-1)}{2f_B} & \text{for } N_B \text{ odd.} \end{cases} \tag{74}$$

Next, we introduce some auxiliary parameters that help us to obtain compact expressions, because the number of parameters is growing dramatically in the three dimensional case.

Definition. *Let*

$$n(k,\lambda_1,\lambda_2) = \begin{cases} (\lambda_1 + 2\lambda_2)N_B - k & \text{if } N_B \text{ even}, k \text{ even}, \\ (\lambda_1 + 2\lambda_2 + 1)N_B - k & \text{if } N_B \text{ even}, k \text{ odd}, \\ (\lambda_1 + \lambda_2)N_B - 2k & \text{if } N_B \text{ odd}, \end{cases}$$

$$m(k,\lambda_1,\lambda_2) = \begin{cases} \frac{k}{2} - (\lambda_1 + \lambda_2)(N_B - 1) & \text{if } N_B \text{ even}, \\ & \quad k \text{ even}, \\ \frac{k}{2} - (\lambda_1 + \lambda_2 + \frac{1}{2})(N_B - 1) & \text{if } N_B \text{ even}, \\ & \quad k \text{ odd} \\ k - (\lambda_1 + \frac{\lambda_2}{2})(N_B - 1) & \text{if } N_B \text{ odd}, \end{cases}$$

$$\ell(k,\lambda_2) = \begin{cases} \frac{k}{2} - \lambda_2(N_B + 1) & \text{if } N_B \text{ even}, k \text{ even}, \\ \frac{k}{2} - (\lambda_2 + \frac{1}{2})(N_B + 1) & \text{if } N_B \text{ even}, k \text{ odd}, \\ k - \frac{\lambda_2}{2}(N_B + 1) & \text{if } N_B \text{ odd}. \end{cases} \tag{75}$$

Given the above definitions, we can now formulate the following theorem for three-dimensional Lissajous-FFP trajectory based MPI:

Theorem 7.1. *The Fourier series coefficients $\boldsymbol{s}_k : \mathbb{R}^3 \to \mathbb{C}^3$ of the MPI system function for a three-dimensional Lissajous FFP-trajectory with the phase offsets $\varphi_x = \varphi_y = \varphi_z = 0$ and $k \in \mathbb{Z}\backslash\{0\}$ can be expressed in terms of tensor products of $V_\ell : \mathbb{R} \to \mathbb{R}$ convolved along the spatial dimensions with the spatial derivative of the Langevin function*

$\mathscr{L}:\mathbb{R}^3\to\mathbb{R}^3$ *by*

$$\begin{aligned}\boldsymbol{s}_k(\boldsymbol{x}) = \sum_{\lambda_1,\lambda_2\in\mathbb{Z}} \frac{(-\mathrm{i})^{\lambda_1+1}\omega_k}{\pi^3}\frac{\operatorname{sgn}(A_xA_yA_z)}{\operatorname{sgn}(G_xG_yG_z)} \\ \int_{\mathbb{R}^3}\left[\frac{\partial^3}{\partial z_1\partial z_2\partial z_3}\mathscr{L}\left(\beta G_x z_1,\beta G_y z_2,\beta G_z z_3\right)\right]_{\substack{z_1=x_1-u_1\\ z_2=x_2-u_2\\ z_3=x_3-u_3}} \\ \cdot V_{n(k,\lambda_1,\lambda_2)}\left(\frac{G_x}{A_x}u_1\right)V_{m(k,\lambda_1,\lambda_2)}\left(\frac{G_y}{A_y}u_2\right) \\ \cdot V_{\ell(k,\lambda_2)}\left(\frac{G_z}{A_z}u_3\right)d\boldsymbol{u},\end{aligned} \tag{76}$$

where

$$V_n(x) = \begin{cases}\operatorname{rect}\left(\frac{x}{2}\right)\left(-\frac{U_{|n|-1}(x)\sqrt{1-x^2}}{|n|}\right) & \text{if } |n|>0\\ \frac{\pi}{2}\operatorname{sgn}(x+1)-\operatorname{rect}\left(\frac{x}{2}\right)\arccos(x) & \text{if } n=0\end{cases} \tag{77}$$

and $U_{n-1}(x)$ denotes the Chebyshev polynomial of second kind and order $n-1$.

Equivalently, the spatial Fourier domain representation of $\boldsymbol{s}_k(\boldsymbol{x})$ can be expressed by

$$\begin{aligned}\hat{\boldsymbol{s}}_k(\boldsymbol{\omega}_{\boldsymbol{x}}) = \sum_{\lambda_1,\lambda_2\in\mathbb{Z}} \frac{(-1)^{\lambda_1+1}\mathrm{i}\omega_k}{|\det(\beta\boldsymbol{G})|}\hat{\mathscr{L}}\left(\frac{\omega_{x_1}}{\beta G_x},\frac{\omega_{x_2}}{\beta G_y},\frac{\omega_{x_3}}{\beta G_z}\right) \\ \cdot J_{n(k,\lambda_1,\lambda_2)}\left(\omega_{x_1}\frac{A_x}{G_x}\right)J_{m(k,\lambda_1,\lambda_2)}\left(\omega_{x_2}\frac{A_y}{G_y}\right) \\ \cdot J_{\ell(k,\lambda_2)}\left(\omega_{x_3}\frac{A_z}{G_z}\right),\end{aligned} \tag{78}$$

where $J_n(\omega_x)$ denotes the n-th Bessel function of first kind and $\hat{\mathscr{L}}:\mathbb{R}^3\to\mathbb{C}^3$ is given by

$$\hat{\mathscr{L}}(\boldsymbol{\omega}_{\boldsymbol{x}}) = -4\pi^2\mathrm{i}\frac{(\pi\|\boldsymbol{\omega}_{\boldsymbol{x}}\|+1)\mathrm{e}^{\pi\|\boldsymbol{\omega}_{\boldsymbol{x}}\|}-1}{\|\boldsymbol{\omega}_{\boldsymbol{x}}\|^2\left(\mathrm{e}^{\pi\|\boldsymbol{\omega}_{\boldsymbol{x}}\|}-1\right)^2}\frac{\boldsymbol{\omega}_{\boldsymbol{x}}}{\|\boldsymbol{\omega}_{\boldsymbol{x}}\|}. \tag{79}$$

For $k=0$ it holds that $\boldsymbol{s}_0(\boldsymbol{x})=\boldsymbol{0}$ and $\hat{\boldsymbol{s}}_0(\boldsymbol{\omega}_{\boldsymbol{x}})=\boldsymbol{0}$.

The proof of the above theorem is given in several steps. First, we state the manifold constraint on variables $m,n,\ell,k,N_B,\lambda_1,\lambda_2$, and then we derive the mapping function $P(\boldsymbol{\omega}_{\boldsymbol{x}},k)$.

Lemma 7.2. *In three dimensional MPI there are two different manifold constrains, depending on $N_B\in\mathbb{N}$ and $k\in\mathbb{Z}$ for $n,m,\ell\in\mathbb{Z}$ with $\lambda_1,\lambda_2\in\mathbb{Z}$*

1. *If N_B is even, the constraint*

$$k=(N_B+1)(N_B-1)n+N_B(N_B+1)m+N_B(N_B-1)\ell$$

is fulfilled for k even by the line equation

$$\begin{pmatrix}n\\m\\\ell\end{pmatrix} = \begin{pmatrix}-k\\ \frac{k}{2}\\ \frac{k}{2}\end{pmatrix}+\lambda_1\begin{pmatrix}N_B\\-(N_B-1)\\0\end{pmatrix}+\lambda_2\begin{pmatrix}2N_B\\-(N_B-1)\\-(N_B+1)\end{pmatrix}, \tag{80}$$

and for k odd we have

$$\begin{aligned}\begin{pmatrix}n\\m\\\ell\end{pmatrix} = \begin{pmatrix}-k\\ \frac{k}{2}\\ \frac{k}{2}\end{pmatrix}+\lambda_1\begin{pmatrix}N_B\\-(N_B-1)\\0\end{pmatrix} \\ +\left(\lambda_2+\frac{1}{2}\right)\begin{pmatrix}2N_B\\-(N_B-1)\\-(N_B+1)\end{pmatrix}.\end{aligned} \tag{81}$$

2. *If N_B is odd, the constraint*

$$2k=(N_B+1)(N_B-1)n+N_B(N_B+1)m+N_B(N_B-1)\ell$$

is fulfilled by

$$\begin{pmatrix}n\\m\\\ell\end{pmatrix} = \begin{pmatrix}-2k\\k\\k\end{pmatrix}+\lambda_1\begin{pmatrix}N_B\\-(N_B-1)\\0\end{pmatrix}+\frac{\lambda_2}{2}\begin{pmatrix}2N_B\\-(N_B-1)\\-(N_B+1)\end{pmatrix}. \tag{82}$$

Because the proof is quite technical and long, the reader is directed to Appendix D for the proof.

Lemma 7.3. *The mapping function $P:\mathbb{R}^3\times\mathbb{Z}\to\mathbb{C}$ for the three-dimensional FFP-Lissajous trajectory $\boldsymbol{x}_{\mathrm{FFP}}:\mathbb{R}\to\mathbb{R}^3$ is given by*

$$\begin{aligned}P(\boldsymbol{\omega}_{\boldsymbol{x}},k) = \sum_{\lambda_1,\lambda_2\in\mathbb{Z}} J_{n(k,\lambda_1,\lambda_2)}\left(\omega_{x_1}\frac{A_x}{G_x}\right)J_{m(k,\lambda_1,\lambda_2)}\left(\omega_{x_2}\frac{A_y}{G_y}\right) \\ \cdot J_{\ell(k,\lambda_2)}\left(\omega_{x_3}\frac{A_z}{G_z}\right)\cdot\mathrm{e}^{\mathrm{i}(n(k,\lambda_1,\lambda_2)\varphi_x+m(k,\lambda_1,\lambda_2)\varphi_y+\ell(k,\lambda_2)\varphi_z)}.\end{aligned} \tag{83}$$

Proof. For an even N_B we have

$$\begin{aligned}P(\boldsymbol{\omega}_{\boldsymbol{x}},k) &= \frac{1}{2\pi}\sum_{n,m,\ell\in\mathbb{Z}}\Bigg[\mathrm{e}^{\mathrm{i}(n\varphi_x+m\varphi_y+\ell\varphi_z)} \\ &\quad J_n\left(\omega_{x_1}\frac{A_x}{G_x}\right)J_m\left(\omega_{x_2}\frac{A_y}{G_y}\right)J_\ell\left(\omega_{x_3}\frac{A_z}{G_z}\right) \\ &\quad \int_{-\pi}^{\pi}\mathrm{e}^{\mathrm{i}[n(N_B-1)(N_B+1)+mN_B(N_B+1)+\ell N_B(N_B-1)-k]z}\,dz\Bigg] \\ &= \sum_{n,m,\ell\in\mathbb{Z}}\Bigg[\mathrm{e}^{\mathrm{i}(n\varphi_x+m\varphi_y+\ell\varphi_z)} \\ &\quad J_n\left(\omega_{x_1}\frac{A_x}{G_x}\right)J_m\left(\omega_{x_2}\frac{A_y}{G_y}\right)J_\ell\left(\omega_{x_3}\frac{A_z}{G_z}\right) \\ &\quad \delta_{(n(N_B+1)(N_B-1)+mN_B(N_B+1)+\ell N_B(N_B-1),k)}\Bigg],\end{aligned}$$

whereas for an odd N_B we obtain

$$\begin{aligned}P(\boldsymbol{\omega}_{\boldsymbol{x}},k) = \sum_{n,m,\ell\in\mathbb{Z}}\Bigg[\mathrm{e}^{\mathrm{i}(n\varphi_x+m\varphi_y+\ell\varphi_z)} \\ J_n\left(\omega_{x_1}\frac{A_x}{G_x}\right)J_m\left(\omega_{x_2}\frac{A_y}{G_y}\right)J_\ell\left(\omega_{x_3}\frac{A_z}{G_z}\right) \\ \delta_{((n(N_B+1)(N_B-1)+mN_B(N_B+1)+\ell N_B(N_B-1)),2k)}\Bigg].\end{aligned}$$

To simplify the expression, we choose the phase offsets to be $\varphi_x = \varphi_y = \varphi_z = 0$ in the following. The argument of the Kronecker symbol follows the constraints in Lemma 7.2. □

The correctness of the frequency-domain representation in (78) can be observed using the same arguments as in the proof of Theorem 5.1 (see (59), (60), (61)) while using the additional relationship $(-1)^{n(k,\lambda_1,\lambda_2)+m(k,\lambda_1,\lambda_2)+\ell(k,\lambda_2)} = (-1)^{\lambda_1}$.

Making use of Lemma 4.11 and assuming that $|k| > 0$, we can give an upper bound for the L^1-norm of $\hat{s}_{\nu k}(\boldsymbol{\omega}_x)$. By combining all factors into a constant $C_2 > 0$, it can be shown that

$$\begin{aligned}\|\hat{s}_{\nu k}\|_{L^1} \leq C_2 \sum_{\lambda_1,\lambda_2\in\mathbb{Z}} &\frac{1}{\max(1,|n(\lambda_1,\lambda_2,k)|^{\frac{4}{3}})} \\ &\cdot \frac{1}{\max(1,|\ell(\lambda_2,k)|^{\frac{4}{3}})\max(1,|m(\lambda_1,\lambda_2,k)|^{\frac{4}{3}})} \\ &< \infty,\end{aligned}$$

where we used the fact that for $k > 0$ there are no $\lambda_1, \lambda_2 \in \mathbb{Z}$ such that $|\ell(\lambda_2,k)| = |m(\lambda_1,\lambda_2,k)| = |n(\lambda_1,\lambda_2,k)| = 0$. Similar to the 2D case, by assuming a zero mean voltage signal, we may set $\boldsymbol{s}_0(\boldsymbol{x}) = \boldsymbol{0}$ and $\hat{\boldsymbol{s}}_0(\boldsymbol{\omega}_x) = \boldsymbol{0}$. Thus, altogether, the series is well defined and the system function $\hat{\boldsymbol{s}}_k(\boldsymbol{\omega}_x)$ is in $L^1(\mathbb{R}^3)$, so that an inverse Fourier transform exists. Analog to Section VI, we can make use of Lemma 4.13 and obtain for the inverse Fourier transform of $\hat{\boldsymbol{s}}_k(\boldsymbol{\omega}_x)$ the expression in (76). Thus, Theorem 7.1 is finally proven.

VIII. Numerical Evaluation

We evaluated the two-dimensional excitation model from Section VI for the system function on the x-receive channel. To approximate the infinite series in (64) we calculated

$$\lambda^* = \arg\min_{\lambda} |k - \lambda N_B| + |k - \lambda(N_B - 1)|$$

corresponding to the minimal mixing order and then

$$\begin{aligned}\boldsymbol{s}_k(\boldsymbol{x}) \approx \sum_{\lambda=-60+\lambda^*}^{60+\lambda^*} &\frac{(-\mathrm{i})^{\lambda+1}\omega_k}{\pi^2} \\ &\int_{\mathbb{R}^2} \left[\frac{\partial^2}{\partial z_1 \partial z_2} \mathscr{L}\left(\beta \boldsymbol{G}\begin{pmatrix} z_1 \\ z_2 \\ x_3 - \frac{c_z}{G_z}\end{pmatrix}\right)\right]_{\substack{z_1=x_1-u_1 \\ z_2=x_2-u_2}} \cdot \\ &V_{-k+\lambda N_B}\left(\frac{G_x}{A_x}u_1\right) V_{k-\lambda(N_B-1)}\left(\frac{G_y}{A_y}u_2\right) du_1\, du_2.\end{aligned} \tag{84}$$

Table 1 defines all additional simulation parameters. For the simulation of the temporal model in (7), we sampled along the temporal dimension with the sampling distance Δt for one period of the FFP trajectory, resulting in 6001 taps. In a next step, we approximated the frequency components by using the discrete Fourier transform $s_k^{\mathrm{FFT}}(\boldsymbol{x}_n)$, where only frequencies up to $k = 1000$ were included. The spatial sampling for the temporal model was performed with the spatial sampling distance $\Delta_1 x_i$, resulting in a grid of size 365×365 in the field of view (FOV).

Table 1: Parameters inside the numerical validation

Parameter		Value
Vacuum permeability	μ_0	$4\pi \cdot 10^{-7}$ H/m
Boltzmann constant	k_B	$1.380649 \cdot 10^{-23}$ J/K
Particle		
Particle core diameter	D	30 nm
Particle core volume	V_c	$\frac{\pi}{6}D^3$
Temperature	T	293 K
Sat. magnetization	M_c	474000 J/m^3/T
	β	$\frac{\mu_0 V_c M_c}{k_B T}$
Scanner Parameter		
Gradient strength	$G_{\{x,y\}}$	$1\ \mathrm{T/m}/\mu_0$
	G_z	$-2\ \mathrm{T/m}/\mu_0$
Excitation amplitudes	$A_{\{x,y\}}$	$0.0125\ \mathrm{T}/\mu_0$
Excitation frequencies	f_x	$2.5/96 \cdot 10^6$ Hz
	f_y	$2.5/93 \cdot 10^6$ Hz
FFP Duration	T_D	$1.1904 \cdot 10^{-3}$ s
Simulation		
FOV		$[-12.5, 12.5]^2$ mm^2
Area in simulation		$[-32.5, 32.5]^2$ mm^2
Temporal sampling	Δt	$2 \cdot 10^{-7}$ s
Spatial sampling	$\Delta_1 x_i$	$6.36 \cdot 10^{-2}$ mm
	$\Delta_2 x_i$	$7.95 \cdot 10^{-3}$ mm
Max. frequency index	$k_{\max}$	1000

The frequency model (84) ($s_k^{\mathrm{approx}}(\boldsymbol{x}_\ell)$) was simulated up to $k = 1000$ with the spatial sampling distance $\Delta_2 x_i$, which was an 8 times finer grid than for sampling with $\Delta_1 x_i$. This was done to reduce the errors due to the discretization of the convolution integral in (84). The convolution was simulated in the range of $[-32.5, 32.5]^2$ mm^2. This helped us to avoid errors at the boundaries of the FOV in the simulation. Afterwards, we downsampled and cropped the area of our approximation so that the new model $s_k^{\mathrm{approx}}(\boldsymbol{x}_n)$ was matched to $s_k^{\mathrm{FFT}}(\boldsymbol{x}_n)$.

Last but not least, we simulated also the spatial frequency model (66) using the two-dimensional Fourier transform of the Langevin function from Appendix E. Spatial frequencies were considered in the range of ± 7860.3 cycles/m in each dimension. The model was discretized to 6133×6133 sampling points. Afterwards, we transformed the approximation back into the spatial domain and matched the spatial positions against $s_k^{\mathrm{FFT}}(\boldsymbol{x})$.

To obtain an objective quality criterion, we calculated the average relative error with respect to the temporal

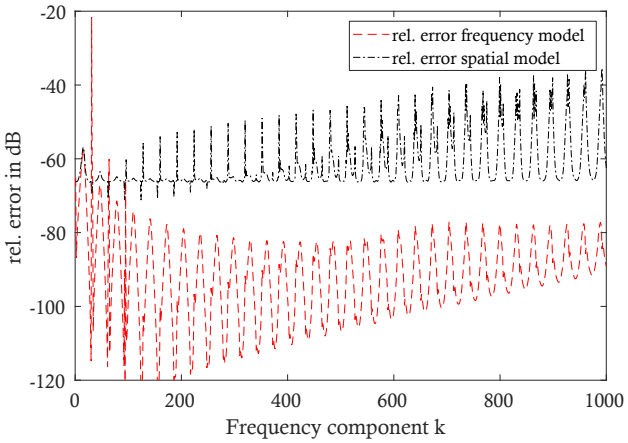

Figure 1: The mean relative error (rel. error) of the frequency components for the frequency model (66) and the spatial model (84) with respect to $s_k^{\mathrm{FFT}}(\boldsymbol{x}_n)$ derived from the temporal model (7).

model (7) for the other two models:

$$\mathrm{MeRE}(k) = \sqrt{\frac{\sum_n \left| s_k^{\mathrm{FFT}}(\boldsymbol{x}_n) - s_k^{\mathrm{approx}}(\boldsymbol{x}_n) \right|^2}{\sum_n \left| s_k^{\mathrm{FFT}}(\boldsymbol{x}_n) \right|^2}},$$

where $s_k^{\mathrm{approx}}(\boldsymbol{x}_n)$ either stems from the model (84) or from (66). In Figure 1 we show the results for all k up to $k = 1000$ in dB. It can be noticed that the errors for both models are generally quite small. They usually range between -100 and -40 dB. The relative error (rel. error) increases as the temporal frequency index k increases. It turned out that the simulation of the frequency model generally had a much lower relative error than the simulated convolution with the Chebyshev polynomials in the spatial domain. The reason lies in the high oscillation of the terms $U_n(x)\sqrt{1-x^2}$ for large n. It was found that some frequency components of the frequency model have a high relative error, especially the component $k = 31$. The main reason is the singularity at the spatial frequency $\boldsymbol{\omega}_{\boldsymbol{x}} = \boldsymbol{0}$. Overall, the simulations validate our calculations and show that the temporal, spatial, and frequency models are equivalent.

IX. Conclusions

In this article, a Fourier analysis of physical MPI models that are based on the Langevin theory of paramagnetism has been presented. The developed mathematical descriptions provides new insights into the MPI imaging process. Possibly, also new reconstruction methods that work on the basis of Bessel functions of first kind can be developed from the presented results. To illustrate and verify the obtained expressions, simulations have been carried out.

While the results for the one-, two-, and -three-dimensional cases have been presented separately, it is also possible to derive the lower-dimensional cases from the three-dimensional one by setting A_y and/or A_z to zero and using the fact that $J_\ell(0) = \delta_{\ell,0}$. However, when keeping the period length T_D in (74) also for the one- and two-dimensional FFP-trajectories, several frequency components $\hat{\boldsymbol{s}}_k(\boldsymbol{\omega}_{\boldsymbol{x}})$ and $\boldsymbol{s}_k(\boldsymbol{x})$ will become systematically zero, because T_D will contain multiple periods of the lower-dimensional trajectories. The separate presentations in Sections V and VI are therefore more compact.

Although the formulations developed in this work are based on a quite simplified model of MPI, they help us to consolidate the mathematical description of MPI. Many observed phenomena in MPI can be explained or proven using this model. For example, the formulation helps to validate reconstruction strategies based on Chebyshev polynomials and matrix compression strategies [22–25] and explains frequency mixing between spatial and temporal frequencies. Still, many physically relevant aspects are not captured by this model, such as relaxation effects, inhomogeneous magnetic fields, and the fact that the SPIO's diameters in a probe are polydisperse rather than monodisperse. Future work can be directed toward extending the developed model to some of these points. It also seems very important to examine the function $P(\boldsymbol{\omega}_{\boldsymbol{x}}, k)$ in (11) for different FFP-trajectories, because this function plays a central role in the mapping between spatial and temporal frequencies (10).

Acknowledgments

This work was supported by the German Research Foundation under grant number ME 1170/7-1. The authors would like to thank the anonymous reviewers whose suggestions have greatly improved the manuscript. In addition, they would like to thank Prof. Dr. Jürgen Prestin from the Institute of Mathematics of the University of Lübeck for helpful comments on the work.

Appendix A:

Proof of Lemma 4.1. The uniform convergence of the series (18) can be shown with help of the gamma function $\Gamma : \mathbb{C} \to \mathbb{C}$, which is an extension of the factorial function to complex values.

The gamma function is given by

$$\Gamma(z) = \int_0^\infty t^{z-1} \mathrm{e}^{-t}\, dt,$$

and based on this, the digamma function is defined as

$$\psi(z) = \frac{d}{dz} \ln(\Gamma(z)) = \frac{\Gamma'(z)}{\Gamma(z)}.$$

The digamma function has the following properties [13]:

$$\psi(1-z)-\psi(z)=\pi\cot(\pi z)$$
$$\psi(z+1)-\psi(z)=\frac{1}{z}.$$

Using these formulas and subtracting the first from the second equation results in

$$\psi(1-z)-\psi(z+1)=\pi\cot(\pi z)-\frac{1}{z}. \tag{85}$$

If we now use as complex argument $z=\frac{\mathrm{i}x}{\pi}$ $(x\in\mathbb{R})$ and multiply (85) with the factor $\frac{\mathrm{i}}{\pi}$ we get the following representation for the Langevin function:

$$\begin{aligned}\mathscr{L}(x)&=\coth(x)-\frac{1}{x}=\mathrm{i}\cot(\mathrm{i}x)-\frac{1}{x}=\frac{\mathrm{i}}{\pi}\left(\pi\cot(\mathrm{i}x)+\frac{\mathrm{i}\pi}{x}\right)\\&=\frac{\mathrm{i}}{\pi}\left(\pi\cot\left(\pi\frac{\mathrm{i}x}{\pi}\right)-\frac{\pi}{\mathrm{i}x}\right)\\&=\frac{\mathrm{i}}{\pi}\left(\psi\left(1-\frac{\mathrm{i}x}{\pi}\right)-\psi\left(\frac{\mathrm{i}x}{\pi}+1\right)\right).\end{aligned} \tag{86}$$

The digamma function can be expressed by the series expansion [13]:

$$\psi(z+1)=-\gamma+\sum_{k=1}^{\infty}\frac{z}{k(k+z)},\quad z\neq-1,-2,-3,\ldots. \tag{87}$$

By inserting (87) into (86) we get

$$\begin{aligned}\mathscr{L}(x)&=\frac{\mathrm{i}}{\pi}\left(-\gamma+\sum_{k=1}^{\infty}\frac{-\frac{\mathrm{i}x}{\pi}}{k(k-\frac{\mathrm{i}x}{\pi})}+\gamma-\sum_{k=1}^{\infty}\frac{\frac{\mathrm{i}x}{\pi}}{k(k+\frac{\mathrm{i}x}{\pi})}\right)\\&=\frac{\mathrm{i}}{\pi}\left(\sum_{k=1}^{\infty}\frac{-\frac{\mathrm{i}x}{\pi}}{k(k-\frac{\mathrm{i}x}{\pi})}-\sum_{k=1}^{\infty}\frac{\frac{\mathrm{i}x}{\pi}}{k(k+\frac{\mathrm{i}x}{\pi})}\right)\\&=\frac{\mathrm{i}}{\pi}\left[-\frac{\mathrm{i}x}{\pi}\left(\sum_{k=1}^{\infty}\frac{1}{k(k-\frac{\mathrm{i}x}{\pi})}+\sum_{k=1}^{\infty}\frac{1}{k(k+\frac{\mathrm{i}x}{\pi})}\right)\right].\end{aligned} \tag{88}$$

We now use the pointwise convergence to $\mathscr{L}(x)$ in the further derivation of the series expansion. Pointwise convergence is given, because for fixed x, the series in (88) are absolutely convergent. This can easily be proved, since $|\frac{1}{k(k\pm\mathrm{i}x/\pi)}|=\mathcal{O}(\frac{1}{k^2})$ and for such a term a series is absolutely convergent and allows for combining the two series into one:

$$\begin{aligned}\mathscr{L}(x)&=\frac{x}{\pi^2}\left(\sum_{k=1}^{\infty}\frac{1}{k(k-\frac{\mathrm{i}x}{\pi})}+\sum_{k=1}^{\infty}\frac{1}{k(k+\frac{\mathrm{i}x}{\pi})}\right)\\&=\frac{x}{\pi^2}\sum_{k=1}^{\infty}\left(\frac{1}{k(k-\frac{\mathrm{i}x}{\pi})}+\frac{1}{k(k+\frac{\mathrm{i}x}{\pi})}\right)\\&=\frac{x}{\pi^2}\sum_{k=1}^{\infty}\frac{k+\frac{\mathrm{i}x}{\pi}+k-\frac{\mathrm{i}x}{\pi}}{k\left(k-\frac{\mathrm{i}x}{\pi}\right)\left(k+\frac{\mathrm{i}x}{\pi}\right)}=\sum_{k=1}^{\infty}\frac{2x}{\pi^2k^2+x^2}.\end{aligned} \tag{89}$$

Additionally, the series is also uniformly convergent on every finite closed interval $\Omega=[-\alpha,\alpha]$ with $\alpha\in\mathbb{R}$. We prove this by the Weierstrass M-test:

$$\begin{aligned}&\forall k\in\mathbb{N}\quad\forall x\in\Omega\quad\exists c_k>0:\\&|f_k(x)|\leq c_k\wedge\sum_{k=1}^{\infty}c_k<\infty\\&\Rightarrow\sum_{k=1}^{\infty}f_k(x)\text{ is uniformly convergent.}\end{aligned}$$

Now let $f_k(x)=\frac{2x}{\pi^2k^2+x^2}$. Then, due to the antisymmetry $f_k(x)=-f_k(-x)$, it is sufficient to find the maximizer $x_{\max}\in[0,\alpha]$. The function term $f_k(x)$ and its derivatives are

$$f_k(x)=\frac{2x}{\pi^2k^2+x^2},\ f_k'(x)=\frac{2\left(\pi^2k^2-x^2\right)}{(\pi^2k^2+x^2)^2},$$
$$f_k''(x)=\frac{4x\left(x^2-3\pi^2k^2\right)}{(\pi^2k^2+x^2)^3}.$$

For $k\leq K-1\leq\alpha\pi<K$, the maximizer on the interval $[0,\alpha]$ of $\left|f_k(x)\right|$ is $x_{\max}^k=\pi k$. This can be checked by observing that $|f_k'(x_{\max}^k)|=0$ and $f_k''(x_{\max}^k)=\frac{-1}{\pi^4k^4}<0$. For $k\geq K$ it can be verified that for all $\tau\in[0,\alpha]$ we have $f'(\tau)>0$. It follows that the continuous function is strictly increasing on the interval and that the maximal value is reached on the right boundary of the interval: $x_{\max}^k=\alpha$. This gives us the inequality

$$\begin{aligned}\sum_{k=1}^{\infty}|f_k(x)|&=\sum_{k=1}^{K-1}|f_k(x)|+\sum_{k=K}^{\infty}|f_k(x)|\\&\leq\sum_{k=1}^{K-1}\frac{2}{\pi k}+\sum_{k=K}^{\infty}\frac{2\alpha}{\pi^2k^2+\alpha^2}\\&<c+2\alpha\sum_{k=1}^{\infty}\frac{1}{\pi^2k^2+\alpha^2}\quad\text{with}\quad c\in\mathbb{R}\\&<c+2\frac{\alpha}{\pi^2}\sum_{k=1}^{\infty}\frac{1}{k^2}=c+\frac{\alpha}{3}<\infty.\end{aligned}$$

The Weierstrass M-test is fulfilled and it follows that the series is uniformly convergent. Due the pointwise convergence in (89) it is uniformly convergent to $\mathscr{L}(x)$ on every arbitrary finite interval on $\mathbb{R}$. □

Appendix B:

Proof of Lemma 4.8. Without loss of generality, we only consider $\hat{\mathscr{L}}_1(\boldsymbol{\omega}_{\boldsymbol{x}})$ in this proof, as the other components follow equivalently.

Utilizing the integration in spherical coordinates

$$\boldsymbol{\omega}_{\boldsymbol{x}}(s,\varphi,\theta)=\begin{bmatrix}\omega_{x_1}\\\omega_{x_2}\\\omega_{x_3}\end{bmatrix}=\begin{bmatrix}s\sin(\theta)\cos(\varphi)\\s\sin(\theta)\sin(\varphi)\\s\cos(\theta)\end{bmatrix}$$

for all $\ell, m, n \in \mathbb{N}_0$ it holds that

$$\begin{aligned}\int_{\mathbb{R}^3} \left|\omega_{x_1}^{\ell}\omega_{x_2}^{m}\omega_{x_3}^{n}\hat{\mathscr{L}}_1(\boldsymbol{\omega_x})\right| d\boldsymbol{\omega_x} \\ = \int_0^{\infty}\int_0^{\pi}\int_0^{2\pi} \Big|s^{\ell+m+n}\sin^{\ell+m}(\theta)\cos^{\ell}(\varphi)\sin^{m}(\varphi) \\ \cdot\cos^{n}(\theta)\hat{\mathscr{L}}_1\big(\boldsymbol{\omega_x}(s,\varphi,\theta)\big)\Big| s^2\sin(\theta)\, d\varphi\, d\theta\, ds.\end{aligned}$$

Inserting

$$\hat{\mathscr{L}}_1\big(\boldsymbol{\omega_x}(s,\varphi,\theta)\big) = \mathrm{i}\Lambda_3'(s)\sin(\theta)\cos(\varphi),$$

where we use that $\|\boldsymbol{\omega_x}(s,\varphi,\theta)\| = s$, we get

$$\begin{aligned}\int_{\mathbb{R}^3} \left|\omega_{x_1}^{\ell}\omega_{x_2}^{m}\omega_{x_3}^{n}\hat{\mathscr{L}}_1(\boldsymbol{\omega_x})\right| d\boldsymbol{\omega_x} \\ = \int_0^{\infty}\int_0^{\pi}\int_0^{2\pi} \Big|s^{\ell+m+n}\sin^{\ell+m+1}(\theta)\cos^{\ell+1}(\varphi)\sin^{m}(\varphi) \\ \cdot\cos^{n}(\theta)\Lambda_3'(s)\Big| s^2\sin(\theta)\, d\varphi\, d\theta\, ds.\end{aligned}$$

Using the inequalities $|\cos(x)| \le 1$ and $|\sin(x)| \le 1$, which hold for all $x \in \mathbb{R}$, an upper bound for the integral can be given as follows:

$$\begin{aligned}&\int_{\mathbb{R}^3} \left|\omega_{x_1}^{\ell}\omega_{x_2}^{m}\omega_{x_3}^{n}\hat{\mathscr{L}}_1(\boldsymbol{\omega_x})\right| d\boldsymbol{\omega_x} \\ &\le \int_0^{\infty}\int_0^{\pi}\int_0^{2\pi} \Big|s^{\ell+m+n}\Lambda_3'(s)\Big| s^2\sin(\theta)\, d\varphi\, d\theta\, ds \\ &= 4\pi\int_0^{\infty} \Big|s^{\ell+m+n}\Lambda_3'(s)\Big| s^2\, ds.\end{aligned}$$

The calculations for $\nu \in \{1,2,3\}$ follow equivalently. We now have to verify for $\hat{\mathscr{L}}_\nu(\boldsymbol{\omega_x}) \in L^1(\mathbb{R}^3)$ that $\left|s^{\ell+m+n+2}\Lambda_3'(s)\right|$ is absolutely integrable. We first obtain

$$\begin{aligned}&\int_0^{\infty} \left|s^{\ell+m+n+2}\Lambda_3'(s)\right| ds \\ &= 4\pi^2\int_0^{\infty} \left|s^{\ell+m+n}\frac{(\pi s+1)\mathrm{e}^{\pi s}-1}{(\mathrm{e}^{\pi s}-1)^2}\right| ds \\ &= 4\pi^2\int_0^{\infty} \left|s^{\ell+m+n}\frac{((\pi s+1)-\mathrm{e}^{-\pi s})\mathrm{e}^{\pi s}}{\mathrm{e}^{2\pi s}(1-\mathrm{e}^{-\pi s})^2}\right| ds \\ &= 4\pi^2\int_0^{\infty} \left|s^{\ell+m+n}\frac{((\pi s+1)-\mathrm{e}^{-\pi s})\mathrm{e}^{-\pi s}}{(1-\mathrm{e}^{-\pi s})^2}\right| ds.\end{aligned} \tag{90}$$

To simplify the problem, we define $\mu = \ell + m + n$ and investigate under which constraints on $\mu \ge 1$ the function

$$F(s) = \begin{cases} \dfrac{s^{\mu}(\pi s+1-\mathrm{e}^{-\pi s})\mathrm{e}^{-\pi s}}{(1-\mathrm{e}^{-\pi s})^2}, & s \ge 0 \\ 0, & s < 0 \end{cases}$$

is in $L^1(\mathbb{R})$. We first aim to find some bounds and limits for $F(s)$, given $\mu \ge 1$ and $s \ge 0$. Using L'Hospital's rule, it is straightforward to show that

$$\lim_{s\to 0^+} F(s) = 2\frac{\delta_{(\mu,1)}}{\pi},$$

where $\delta_{(\mu,1)}$ denotes the Kronecker delta. This means that the value at zero is well defined. Next, we rewrite $F(s)$ for $s > 0$ as

$$F(s) = \frac{s^{\mu}}{1-\mathrm{e}^{-\pi s}}\left(\frac{\pi s}{1-\mathrm{e}^{-\pi s}}+1\right)\mathrm{e}^{-\pi s}, \qquad s > 0$$

and observe that $F(s) > 0$ for all $s > 0$. To obtain an upper bound on $F(s)$, let us start with the inequality

$$\pi s + 1 < \mathrm{e}^{\pi s}.$$

By multiplying this expression with $\mathrm{e}^{-\pi s}$ and changing the order we get

$$\begin{aligned}\mathrm{e}^{-\pi s}(\pi s+1) &< 1 \\ 0 &< 1-\pi s\mathrm{e}^{-\pi s}-\mathrm{e}^{-\pi s} \\ \pi s &< \pi s+1-\pi s\mathrm{e}^{-\pi s}-\mathrm{e}^{-\pi s} = (\pi s+1)(1-\mathrm{e}^{-\pi s}) \\ \frac{\pi s}{(1-\mathrm{e}^{-\pi s})} &< \pi s+1,\end{aligned}$$

which holds for all $s > 0$. Finally, we obtain the upper bound

$$\begin{aligned}F(s) &< \frac{1}{\pi}s^{\mu-1}(\pi s+1)(\pi s+2)\mathrm{e}^{-\pi s} \\ &< \frac{1}{\pi}(\pi s+2)^{\mu+1}\mathrm{e}^{-\pi s}.\end{aligned}$$

Now we prove that $F(s) \in L^1(\mathbb{R})$ for $\mu \ge 1$. Using the upper bound, we have

$$\int_{-\infty}^{\infty}|F(s)|\, ds < \frac{1}{\pi}\int_0^{\infty}(\pi s+2)^{(\mu+1)}\mathrm{e}^{-\pi s}\, ds.$$

The substitution $z = \pi s + 2$ yields

$$\begin{aligned}\int_{-\infty}^{\infty}|F(s)|\, ds &< \frac{1}{\pi}\int_2^{\infty} z^{\mu+1}\mathrm{e}^{-(z-2)}\frac{dz}{\pi} \\ &= \frac{\mathrm{e}^2}{\pi^2}\int_2^{\infty} z^{\mu+1}\mathrm{e}^{-z}\, dz \\ &\le \frac{\mathrm{e}^2}{\pi^2}\int_0^{\infty} z^{\mu+1}\mathrm{e}^{-z}\, dz = \frac{\mathrm{e}^2\Gamma(\mu+2)}{\pi^2} < \infty.\end{aligned}$$

Thus, $F(s) \in L^1(\mathbb{R})$ for all $\mu \ge 1$. Now, let us consider the original problem (90). From $F(s) \in L^1(\mathbb{R})$ for all $\mu \ge 1$, we can conclude that for $\mu = m+n+\ell \ge 1$ we have $\omega_{x_1}^{\ell}\omega_{x_2}^{m}\omega_{x_3}^{n}\hat{\mathscr{L}}_\nu(\boldsymbol{\omega_x}) \in L^1(\mathbb{R}^3)$. □

Appendix C:

Proof of Lemma 4.12. We aim to prove the convolution correspondence in Lemma 4.12, which helps us to unify the notation in this work. First, we rewrite the left term in (44) with

$$v_0\left(\tfrac{x}{\alpha}\right) = \mathrm{rect}\left(\tfrac{x}{2\alpha}\right)\frac{T_0\left(\frac{x}{\alpha}\right)}{\sqrt{1-\left(\frac{x}{\alpha}\right)^2}}, \qquad \alpha \neq 0$$

from (35) as

$$\int_{-\infty}^{\infty} F(x-y)\frac{1}{|\alpha|}\operatorname{rect}\left(\frac{y}{2\alpha}\right)\frac{1}{\sqrt{1-\left(\frac{y}{\alpha}\right)^2}}\,dy = \int_{-|\alpha|}^{|\alpha|} F(x-y)\frac{1}{|\alpha|}\frac{1}{\sqrt{1-\left(\frac{y}{\alpha}\right)^2}}\,dy$$

Partial integration yields

$$\begin{aligned}
&\int_{-|\alpha|}^{|\alpha|} F(x-y)\frac{1}{|\alpha|}\frac{1}{\sqrt{1-\left(\frac{y}{\alpha}\right)^2}}\,dy \\
&\quad= F(x-y)\frac{\alpha}{|\alpha|}\arcsin\left(\frac{y}{\alpha}\right)\Big|_{-|\alpha|}^{|\alpha|} \\
&\qquad+\int_{-|\alpha|}^{|\alpha|} f(x-y)\frac{\alpha}{|\alpha|}\arcsin\left(\frac{y}{\alpha}\right)\,dy \\
&\quad= \frac{\pi}{2}\left(F(x-|\alpha|)+F(x+|\alpha|)\right) \\
&\qquad+\int_{-|\alpha|}^{|\alpha|} f(x-y)\frac{\alpha}{|\alpha|}\arcsin\left(\frac{y}{\alpha}\right)\,dy.
\end{aligned} \tag{91}$$

Now notice that because of $\lim_{x\to\pm\infty} F(x) = \pm c$ with $c \in \mathbb{R}$ and $F(x) \in L^\infty(\mathbb{R})$, it holds that

$$\begin{aligned}
&\int_{-\infty}^{\infty} f(x-\tau)\operatorname{sgn}(\tau-y)\,d\tau \\
&= \int_{y}^{\infty} f(x-\tau)d\tau - \int_{-\infty}^{y} f(x-\tau)d\tau \\
&= -F(x-\tau)\Big|_{\tau=y}^{\infty} + F(x-\tau)\Big|_{\tau=-\infty}^{y} \\
&= 2F(x-y) - \underbrace{\lim_{\tau\to\infty}\left[F(x-\tau)+F(x+\tau)\right]}_{=0} = 2F(x-y).
\end{aligned}$$

Using this relationship inside the convolution integral in (91), we get

$$\begin{aligned}
&\int_{-\infty}^{\infty} F(x-y)\frac{1}{|\alpha|}v_0\left(\frac{y}{\alpha}\right)\,dy \\
&= \int_{-\infty}^{\infty} f(x-y)\left(\frac{\pi}{4}\left(\operatorname{sgn}(y-|\alpha|)+\operatorname{sgn}(y+|\alpha|)\right)\right. \\
&\qquad\left.+\operatorname{rect}\left(\frac{y}{2\alpha}\right)\frac{\alpha}{|\alpha|}\arcsin\left(\frac{y}{\alpha}\right)\right)dy.
\end{aligned}$$

The term

$$\frac{\pi}{4}\left(\operatorname{sgn}(y-|\alpha|)+\operatorname{sgn}(y+|\alpha|)\right)+\operatorname{rect}\left(\frac{y}{2\alpha}\right)\frac{\alpha}{|\alpha|}\arcsin\left(\frac{y}{\alpha}\right)$$

is is equivalent to

$$\begin{aligned}
&\frac{1}{\operatorname{sgn}(\alpha)}\left(\frac{\pi}{2}\operatorname{sgn}\left(\frac{y}{\alpha}+1\right)-\operatorname{rect}\left(\frac{y}{2\alpha}\right)\arccos\left(\frac{y}{\alpha}\right)\right) \\
&=\frac{1}{\operatorname{sgn}(\alpha)}V_0\left(\frac{y}{\alpha}\right)
\end{aligned}$$

with $\operatorname{sgn}(\alpha) = \frac{\alpha}{|\alpha|} = \frac{|\alpha|}{\alpha}$. Thus, we have obtained the expression on the right-hand side of (44). □

Appendix D:

Proof of Lemma 7.2. We aim to prove the constraints on n, m, ℓ for three-dimensional MPI formulated in Lemma 7.2. For this, we need to distinguish between different cases.

Case 1: N_B even The following manifold condition has to hold:

$$k = \begin{pmatrix}(N_B+1)(N_B-1), & N_B(N_B+1), & N_B(N_B-1)\end{pmatrix}\begin{pmatrix} n \\ m \\ \ell \end{pmatrix} \tag{92}$$

with $k, \ell, m, n \in \mathbb{Z}$. This constraint means that all points (m, n, ℓ) are lying on a plane inside a three-dimensional space. We can verify that

$$\begin{aligned}
\begin{pmatrix} n \\ m \\ \ell \end{pmatrix} &= \begin{pmatrix} -k \\ \frac{k}{2} \\ \frac{k}{2} \end{pmatrix} + \lambda_1 \begin{pmatrix} N_B \\ -(N_B-1) \\ 0 \end{pmatrix} \\
&\quad + (\lambda_2+\alpha)\begin{pmatrix} 2N_B \\ -(N_B-1) \\ -(N_B+1) \end{pmatrix}
\end{aligned} \tag{93}$$

with $\alpha \in \left\{0, \frac{1}{2}\right\}$ and $\lambda_1, \lambda_2 \in \mathbb{Z}$ is a valid solution that fulfills (92) by inserting (93) into (92):

$$\begin{aligned}
&\begin{pmatrix}(N_B+1)(N_B-1), & N_B(N_B+1), & N_B(N_B-1)\end{pmatrix}\begin{pmatrix} n \\ m \\ \ell \end{pmatrix} \\
&= -k(N_B+1)(N_B-1) + \frac{k}{2}N_B(N_B+1) + \frac{k}{2}N_B(N_B-1) \\
&\quad + \lambda_1\underbrace{\left((N_B+1)(N_B-1)N_B + N_B(N_B+1)(-(N_B-1))\right)}_{=0} \\
&\quad + (\lambda_2+\alpha)\Big[(N_B+1)(N_B-1)2N_B \\
&\qquad + N_B(N_B+1)(-(N_B-1)) + N_B(N_B-1)(-(N_B+1))\Big] \\
&= \underbrace{-k(N_B^2-1) + \frac{k}{2}(N_B^2+N_B) + \frac{k}{2}(N_B^2-N_B)}_{=k} \\
&\quad + (\lambda_2+\alpha)\underbrace{\left[(N_B^2-1)2N_B - (N_B^2-1)N_B - N_B(N_B^2-1)\right]}_{=0} \\
&= k.
\end{aligned}$$

This means that the constraint (92) is fulfilled for both even and odd k in (80) and (81), respectively. According to (93), for even k and $\alpha = 0$ as well as for odd k and $\alpha = \frac{1}{2}$, we have $\lambda_1, \lambda_2 \in \mathbb{Z}$ and $n, m, \ell \in \mathbb{Z}$. The general case with $\lambda_i \in \mathbb{R}$ can be expressed as $\lambda_i = \tilde{\lambda}_i + \beta_i$ with $\tilde{\lambda}_i \in \mathbb{Z}$ and $\beta_i \in (0, 1)$. Now, we differentiate between $k \in \mathbb{Z}$ even and odd.

1. k even and $\alpha = 0$: It is sufficient to check for which

β_i the following constraints are fulfilled:

$$(\beta_1+2\beta_2)N_B\in\mathbb{Z}, \tag{94}$$
$$-(\beta_1+\beta_2)(N_B-1)\in\mathbb{Z}, \tag{95}$$
$$-\beta_2(N_B+1)\in\mathbb{Z}. \tag{96}$$

By adding up (94) and (95) and rearranging the obtained equation we get

$$\beta_1+\underbrace{\beta_2(N_B+1)}_{\text{by (96)}\in\mathbb{Z}}\in\mathbb{Z}. \tag{97}$$

Consequently, only $\beta_1=0$ or $\beta_1=1$ are valid solutions. By subtracting (96) from (95) and setting $\beta_1=0$ we get

$$2\beta_2\in\mathbb{Z}, \tag{98}$$

which only allows a solution with $\beta_2\in\{0,\frac{1}{2},1\}$.

Utilizing that N_B is even, we have $\beta_2 N_B\in\mathbb{Z}$ and consequently we get from (96)

$$-\beta_2(N_B+1)=-\beta_2N_B-\beta_2\in\mathbb{Z}\Rightarrow-\beta_2\in\mathbb{Z}.$$

This means that $\beta_2=0$ or $\beta_2=1$ are the only valid solutions. Therefore, there is no $\beta_1,\beta_2\in(0,1)$ such that $n,m,\ell\in\mathbb{Z}$.

2. k odd and $\alpha=\frac{1}{2}$: Here, using that $\frac{N_B}{2}\in\mathbb{Z}$, (93) results in the following constraints:

$$(\beta_1+2\beta_2)N_B\in\mathbb{Z} \tag{99}$$
$$-(\beta_1+\beta_2)(N_B-1)\in\mathbb{Z} \tag{100}$$
$$-\beta_2(N_B+1)\in\mathbb{Z}. \tag{101}$$

These are exactly the same constraints as (94), (95), and (96). Consequently, the constraints on β_1 and β_2 are also the same.

Case 2: N_B odd To derive the manifold conditions for the case where N_B is odd, we set

$$2k=\big((N_B+1)(N_B-1),\quad N_B(N_B+1),\quad N_B(N_B-1)\big)\begin{pmatrix}n\\m\\\ell\end{pmatrix}. \tag{102}$$

It can easily be shown that a possible solution is given for $n=-2k$, $m=k$ and $\ell=k$. The basis vectors are the same as for even N_B, and we can write the possible solutions as

$$\begin{pmatrix}n\\m\\\ell\end{pmatrix}=\begin{pmatrix}-2k\\k\\k\end{pmatrix}+\lambda_1\begin{pmatrix}N_B\\-(N_B-1)\\0\end{pmatrix}+\frac{\lambda_2}{2}\begin{pmatrix}2N_B\\-(N_B-1)\\-(N_B+1)\end{pmatrix}.$$

The fact that $\lambda_1,\lambda_2\in\mathbb{Z}$ holds can be concluded from the three constraints

$$(\lambda_1+\lambda_2)N_B\in\mathbb{Z}, \tag{103}$$
$$-\left(\lambda_1+\frac{\lambda_2}{2}\right)(N_B-1)\in\mathbb{Z}, \tag{104}$$
$$-\frac{\lambda_2}{2}(N_B+1)\in\mathbb{Z}. \tag{105}$$

By adding up (103) and (104) and rearranging the obtained equation we get

$$\underbrace{(N_B+1)\frac{\lambda_2}{2}}_{\in\mathbb{Z}\text{ due to (105)}}+\lambda_1\in\mathbb{Z}.$$

Consequently, $\lambda_1\in\mathbb{Z}$. By subtracting (105) from (104) and setting $\lambda_1=0$ we get

$$\lambda_2\in\mathbb{Z}. \qquad \square$$

Appendix E:

In the following, the two-dimensional Fourier transforms of $\ell_{\mathrm{n}}:\mathbb{R}^2\to\mathbb{R}$ with $\ell_{\mathrm{n}}(\boldsymbol{x})=\mathscr{L}_{\mathrm{n}}(\|\boldsymbol{x}\|)$ and $\mathscr{L}:\mathbb{R}^2\to\mathbb{R}$ are calculated, and it is shown how they can be treated numerically. To simplify the calculations, we use the Hankel transform, which is closely related to the n-dimensional Fourier transform of rotational invariant functions [26]. The Hankel transform with order $\mu>-\frac{1}{2}$ of a function $g:\mathbb{R}_+\to\mathbb{R}$ is defined as

$$g_\mu(s)=\mathscr{H}_\mu\big[g(r)\big]=\int_0^\infty J_\mu(sr)g(r)r\,dr,$$

where $J_\mu(s)$ denotes the μ-th Bessel function of first kind. Now let $f:\mathbb{R}^n\to\mathbb{R}$ be a rotational invariant function, so that

$$f(\boldsymbol{x})=F(\|\boldsymbol{x}\|)=F(r),$$

where $F:\mathbb{R}_+\to\mathbb{R}$ denotes a one-dimensional function. Then we have for the Fourier transform

$$\hat{f}(\boldsymbol{\omega_x})=\hat{F}_n(s)=\hat{F}_n(\|\boldsymbol{\omega_x}\|)$$

with

$$\hat{F}_n(s)=(2\pi)^{\frac{n}{2}}\,s^{-\frac{n-2}{2}}\,\mathscr{H}_{\frac{n-2}{2}}\Big[r^{\frac{n-2}{2}}F(r)\Big].$$

For the special case of $n=2$ we state the expressions explicitly. For $n=2$ we obtain

$$\hat{F}_2(s)=2\pi\mathscr{H}_0[F(r)]=2\pi\int_0^\infty J_0(sr)F(r)r\,dr,$$

where the zeroth order Hankel transform of $\mathscr{L}_\mathrm{n}(r)$ reads

$$\begin{aligned}\mathscr{H}_0[\mathscr{L}_\mathrm{n}(r)] &= \mathscr{H}_0\left[\sum_{k=1}^{\infty}\frac{2}{k^2\pi^2+r^2}\right] = \sum_{k=1}^{\infty}\mathscr{H}_0\left[\frac{2}{k^2\pi^2+r^2}\right] \\ &= \sum_{k=1}^{\infty} 2K_0(k\pi s) = 2\sum_{k=1}^{\infty}\int_0^{\infty} \mathrm{e}^{-k\pi s\cosh(t)}\,dt \\ &= 2\int_0^{\infty}\sum_{k=1}^{\infty}\mathrm{e}^{-k\pi s\cosh(t)}\,dt \\ &= \int_0^{\infty}\frac{2}{\mathrm{e}^{\pi s\cosh(t)}-1}\,dt\end{aligned}$$

with $K_0(k\pi s)$ being the modified Bessel function of second kind.

Finally, we use the above result to state the rotation-invariant Fourier transforms of $\mathscr{L}_\mathrm{n}(r)$ with $r = \|\boldsymbol{x}\|$ in two-dimensions. For the 2D case, we have

$$\hat{\mathscr{L}}_\mathrm{n}(\boldsymbol{\omega}_{\boldsymbol{x}}) = \Lambda_2(s) = 4\pi\int_0^{\infty}\frac{1}{\mathrm{e}^{\pi s\cosh(t)}-1}\,dt \tag{106}$$

with $s = \|\boldsymbol{\omega}_{\boldsymbol{x}}\|$.

The 2D Fourier transform of the 2D Langevin function is the derivative of (106), multiplied by the normalized vector $\frac{\boldsymbol{\omega}_{\boldsymbol{x}}}{\|\boldsymbol{\omega}_{\boldsymbol{x}}\|}$:

$$\begin{aligned}\hat{\mathscr{L}}(\boldsymbol{\omega}_{\boldsymbol{x}}) &= \mathrm{i}\Lambda_2'(\|\boldsymbol{\omega}_{\boldsymbol{x}}\|)\frac{\boldsymbol{\omega}_{\boldsymbol{x}}}{\|\boldsymbol{\omega}_{\boldsymbol{x}}\|} \\ &= -4\pi^2\mathrm{i}\left(\int_0^{\infty}\frac{\cosh(t)\mathrm{e}^{\pi\|\boldsymbol{\omega}_{\boldsymbol{x}}\|\cosh(t)}}{(\mathrm{e}^{\pi\|\boldsymbol{\omega}_{\boldsymbol{x}}\|\cosh(t)}-1)^2}\,dt\right)\frac{\boldsymbol{\omega}_{\boldsymbol{x}}}{\|\boldsymbol{\omega}_{\boldsymbol{x}}\|} \\ &= \frac{-\pi^2\mathrm{i}\boldsymbol{\omega}_{\boldsymbol{x}}}{\|\boldsymbol{\omega}_{\boldsymbol{x}}\|}\left(\int_0^{\infty}\cosh(t)\operatorname{csch}^2\left(\frac{\pi}{2}\|\boldsymbol{\omega}_{\boldsymbol{x}}\|\cosh(t)\right)dt\right),\end{aligned}$$

where $\operatorname{csch}(x) = \frac{1}{\sinh(x)}$ denotes the hyperbolic cosecant. The last formula can be reformulated by different substitutions. The following two should be noted:

1. The substitution $t = \tanh^{-1}(z)$ yields

$$\hat{\mathscr{L}}(\boldsymbol{\omega}_{\boldsymbol{x}}) = \frac{-\pi^2\mathrm{i}\boldsymbol{\omega}_{\boldsymbol{x}}}{\|\boldsymbol{\omega}_{\boldsymbol{x}}\|}\int_0^1\frac{\operatorname{csch}^2\left(\frac{\frac{1}{2}\pi\|\boldsymbol{\omega}_{\boldsymbol{x}}\|}{\sqrt{1-z^2}}\right)}{(1-z^2)^{\frac{3}{2}}}dz.$$

2. Using the substitution $z = \sin(u)$, we obtain

$$\begin{aligned}\hat{\mathscr{L}}(\boldsymbol{\omega}_{\boldsymbol{x}}) &= \frac{-\pi^2\mathrm{i}\boldsymbol{\omega}_{\boldsymbol{x}}}{\|\boldsymbol{\omega}_{\boldsymbol{x}}\|}\int_0^{\frac{\pi}{2}}\frac{\operatorname{csch}^2\left(\frac{\pi\|\boldsymbol{\omega}_{\boldsymbol{x}}\|}{2\cos(u)}\right)}{\cos^2(u)}du \\ &= \frac{-\pi^2\mathrm{i}\boldsymbol{\omega}_{\boldsymbol{x}}}{\|\boldsymbol{\omega}_{\boldsymbol{x}}\|^3}\int_0^{\frac{\pi}{2}}\Bigg(\|\boldsymbol{\omega}_{\boldsymbol{x}}\|\operatorname{csch}\left(\frac{\pi}{2}\|\boldsymbol{\omega}_{\boldsymbol{x}}\|\sec(u)\right)\cdot \\ &\qquad \sec(u)\Bigg)^2 du,\end{aligned} \tag{107}$$

where $\sec(u) = \frac{1}{\cos(u)}$.

Equation (107) is quite comfortable for numerical integration, because the integrand

$$i(\|\boldsymbol{\omega}_{\boldsymbol{x}}\|, u) = \left(\operatorname{csch}\left(\frac{\pi}{2}\|\boldsymbol{\omega}_{\boldsymbol{x}}\|\sec(u)\right)\sec(u)\right)^2$$

is fully defined for all $\|\boldsymbol{\omega}_{\boldsymbol{x}}\| \neq 0$. It can be shown that

$$\lim_{u^+\to\frac{\pi}{2}} i(\|\boldsymbol{\omega}_{\boldsymbol{x}}\|, u) = 0$$

is the only point singularity on the finite interval $\left[0, \frac{\pi}{2}\right]$, which can be continuously removed. The other formulations have either a non-closed infinite interval, a non-removable singularity at the boundary of the interval, or even both. Moreover, for the numerical integration it is helpful to remove the singularity at $\|\boldsymbol{\omega}_{\boldsymbol{x}}\| = 0$ by multiplying with $\|\boldsymbol{\omega}_{\boldsymbol{x}}\|^2$. This corresponds to a second-order singularity in the integrand $i(\|\boldsymbol{\omega}_{\boldsymbol{x}}\|, u)$, which leads to

$$\lim_{\|\boldsymbol{\omega}_{\boldsymbol{x}}\|\to 0}\|\boldsymbol{\omega}_{\boldsymbol{x}}\|_2^2 i(\|\boldsymbol{\omega}_{\boldsymbol{x}}\|, u) = \frac{4}{\pi^2}.$$

References

[1] T. Kluth. Mathematical models for magnetic particle imaging. *Inverse Problems*, 34(8):083001, 2018, doi:10.1088/1361-6420/aac535.

[2] J. Rahmer, J. Weizenecker, B. Gleich, and J. Borgert. Signal encoding in magnetic particle imaging: properties of the system function. *BMC Medical Imaging*, 9:4, 2009, doi:10.1186/1471-2342-9-4.

[3] P. W. Goodwill and S. M. Conolly. Multidimensional X-Space Magnetic Particle Imaging. *IEEE Transactions on Medical Imaging*, 30(9):1581–1590, 2011, doi:10.1109/TMI.2011.2125982.

[4] J. J. Konkle, P. W. Goodwill, O. M. Carrasco-Zevallos, and S. M. Conolly. Projection Reconstruction Magnetic Particle Imaging. *IEEE Transactions on Medical Imaging*, 32(2):338–347, 2013, doi:10.1109/TMI.2012.2227121.

[5] T. Knopp, S. Biederer, T. F. Sattel, M. Erbe, and T. M. Buzug. Prediction of the spatial resolution of magnetic particle imaging using the modulation transfer function of the imaging process. *IEEE Transactions on Medical Imaging*, 30(6):1284–1292, 2011, doi:10.1109/TMI.2011.2113188.

[6] M. Maass and A. Mertins, On the formulation of the magentic particle imaging system function in Fourier space, in *International Workshop on Magnetic Particle Imaging*, 39–40, 2018.

[7] W. Erb, A. Weinmann, M. Ahlborg, C. Brandt, G. Bringout, T. M. Buzug, J. Frikel, C. Kaethner, T. Knopp, T. März, M. Möddel, M. Storath, and A. Weber. Mathematical analysis of the 1D model and reconstruction schemes for magnetic particle imaging. *Inverse Problems*, 34(5):055012, 2018, doi:10.1088/1361-6420/aab8d1.

[8] A. Cordes and T. M. Buzug, Deconvolution kernel for 1D x-space MPI, in *International Workshop on Magnetic Particle Imaging*, 49–50, 2018.

[9] T. Knopp and T. M. Buzug, Magnetic Particle Imaging: An Introduction to Imaging Principles and Scanner Instrumentation. Berlin, Heidelberg: Springer Berlin Heidelberg, 2012, doi:10.1007/978-3-642-04199-0.

[10] P. Goodwill, G. Scott, P. Stang, and S. Conolly. Narrowband Magnetic Particle Imaging. *IEEE Transactions on Medical Imaging*, 28(8):1231–1237, 2009, doi:10.1109/TMI.2009.2013849.

[11] H. Schomberg, Magnetic particle imaging: Model and reconstruction, in *IEEE International Symposium on Biomedical Imaging: From Nano to Macro*, 992–995, IEEE, 2010. doi:10.1109/ISBI.2010.5490155.

[12] S. Bergner, T. Moller, D. Weiskopf, and D. J. Muraki. A Spectral Analysis of Function Composition and its Implications for Sampling in Direct Volume Visualization. *IEEE Transactions on Visualization and Computer Graphics*, 12(5):1353–1360, 2006, doi:10.1109/TVCG.2006.113.

[13] M. Abramowitz and I. A. Stegun, Eds., Handbook of Mathematical Functions with Formulas, Graphs, and Mathematical Tables, Applied Ma. Washington, D.C.: National Bureau of Standards, 1964,

[14] K. A. Stromberg, An Introduction to Classical Real Analysis. American Mathematical Society Chelsea Publishing, 2015, ISBN: 1470425440.

[15] L. Grafakos and G. Teschl. On Fourier Transforms of Radial Functions and Distributions. *Journal of Fourier Analysis and Applications*, 19(1):167–179, 2013, doi:10.1007/s00041-012-9242-5.

[16] R. Estrada. On Radial Functions and Distributions and Their Fourier Transforms. *Journal of Fourier Analysis and Applications*, 20(2):301–320, 2014, doi:10.1007/s00041-013-9313-2.

[17] H. O. Beća. An orthogonal set based on Bessel functions of the first kind. *Publikacije Elektrotehničkog fakulteta. Serija Matematika i fizika*, 678(715):85–90, 1980.

[18] K. Stempak. A weighted uniform L^p–estimate of Bessel functions: A note on a paper of Guo. *Proceedings of the American Mathematical Society*, 128(10):2943–2946, 2000, doi:10.1090/S0002-9939-00-05365-X.

[19] L. J. Landau. Bessel Functions: Monotonicity and Bounds. *Journal of the London Mathematical Society*, 61(1):197–215, 2000, doi:10.1112/S0024610799008352.

[20] T. März and A. Weinmann. Model-based reconstruction for magnetic particle imaging in 2D and 3D. *Inverse Problems and Imaging*, 10(4):1087–1110, 2016, doi:10.3934/ipi.2016033.

[21] H. Bateman, Higher Transcendental Functions, volume 2, A. Erdélyi, Ed. McGraw-Hill Book Company, Inc., 1953,

[22] J. Lampe, C. Bassoy, J. Rahmer, J. Weizenecker, H. Voss, B. Gleich, and J. Borgert. Fast reconstruction in magnetic particle imaging. *Physics in Medicine and Biology*, 57(4):1113–1134, 2012, doi:10.1088/0031-9155/57/4/1113.

[23] T. Knopp and A. Weber. Local System Matrix Compression for Efficient Reconstruction in Magnetic Particle Imaging. *Advances in Mathematical Physics*, 2015:1–7, 2015, doi:10.1155/2015/472818.

[24] M. Maass, K. Bente, M. Ahlborg, H. Medimagh, H. Phan, T. M. Buzug, and A. Mertins. Optimized Compression of MPI System Matrices Using a Symmetry-Preserving Secondary Orthogonal Transform. *International Journal on Magnetic Particle Imaging*, 2(1), 2016, doi:10.18416/IJMPI.2016.1607002.

[25] L. Schmiester, M. Möddel, W. Erb, and T. Knopp. Direct Image Reconstruction of Lissajous-Type Magnetic Particle Imaging Data Using Chebyshev-Based Matrix Compression. *IEEE Transactions on Computational Imaging*, 3(4):671–681, 2017, doi:10.1109/TCI.2017.2706058.

[26] R. Piessens, Hankel Transform, in *Transforms and Applications Handbook, Third Edition*, A. D. Poularikas, Ed., CRC Press, 2010. doi:10.1201/9781420066531-c9.

